Oleuropein derivatives from olive fruit extracts reduce α-synuclein fibrillation and oligomer toxicity

Received for publication, September 6, 2018, and in revised form, January 9, 2019 Published, Papers in Press, January 17, 2019, DOI 10.1074/jbc.RA118.005723

Hossein Mohammad-Beigi[‡1], Farhang Aliakbari[‡§], Cagla Sahin[‡¶], Charlotte Lomax[‖], Ahmed Tawfike[‖], Nicholas P. Schafer[‡2], Alireza Amiri-Nowdijeh[**], Hoda Eskandari[‡], Ian Max Møller[¶], Mehdi Hosseini-Mazinani[**], Gunna Christiansen[‡‡], Jane L. Ward[‖], Dina Morshedi[§3], and Daniel E. Otzen[‡§§4]

From the [‡]Interdisciplinary Nanoscience Centre (iNANO), Aarhus University, Gustav Wieds Vej 14, DK-8000 Aarhus C, Denmark, the Departments of [§]Industrial and Environmental Biotechnology and [**]Agricultural Biotechnology, National Institute of Genetic Engineering and Biotechnology, P. O. Box 1417863171, Tehran, Iran, the [¶]Department of Molecular Biology and Genetics, Aarhus University, Forsøgsvej 1, DK-4200 Slagelse, Denmark, the [‖]Computational and Analytical Sciences Department, Rothamsted Research, West Common, Harpenden, Herts AL5 2JQ, United Kingdom, the [‡‡]Department of Biomedicine-Medical Microbiology and Immunology, Aarhus University, 8000 Aarhus C, Denmark, and the [§§]Department of Molecular Biology and Genetics, Aarhus University, Gustav Wieds Vej 10C, DK-8000 Aarhus C, Denmark

Edited by Paul E. Fraser

Aggregation of α-synuclein (αSN) is implicated in neuronal degeneration in Parkinson's disease and has prompted searches for natural compounds inhibiting αSN aggregation and reducing its tendency to form toxic oligomers. Oil from the olive tree (*Olea europaea* L.) represents the main source of fat in the Mediterranean diet and contains variable levels of phenolic compounds, many structurally related to the compound oleuropein. Here, using αSN aggregation, fibrillation, size-exclusion chromatography–multiangle light scattering (SEC-MALS)-based assays, and toxicity assays, we systematically screened the fruit extracts of 15 different olive varieties to identify compounds that can inhibit αSN aggregation and oligomer toxicity and also have antioxidant activity. Polyphenol composition differed markedly among varieties. The variety with the most effective antioxidant and aggregation activities, Koroneiki, combined strong inhibition of αSN fibril nucleation and elongation with strong disaggregation activity on preformed fibrils and prevented the formation of toxic αSN oligomers. Fractionation of the Koroneiki extract identified oleuropein aglycone, hydroxyl oleuropein aglycone, and oleuropein as key compounds responsible for the differences in inhibition across the extracts. These phenolic compounds inhibited αSN amyloidogenesis by directing αSN monomers into small αSN oligomers with lower toxicity, thereby suppressing the subsequent fibril growth phase. Our results highlight the molecular consequences of differences in the level of effective phenolic compounds in different olive varieties, insights that have implications for long-term human health.

Parkinson's disease (PD),[5] the second most common neurodegenerative disease, is characterized by the degeneration of dopaminergic neurons in the *substantia nigra pars compacta* due to deposition of intracellular inclusions known as Lewy bodies. These deposits can spread from cell to cell in a prion-like fashion (1–4), leading to rigid posture, uncertain pace, and resting tremor. The major component of Lewy bodies is the 140-residue protein α-synuclein (αSN), which consists of three main regions: an amphiphilic N-terminal part, a nonamyloid hydrophobic β-peptide component (NAC), and an acidic C terminus. The nonamyloid hydrophobic β-peptide component region makes up the fibril core of amyloid fibril (5). Although monomeric αSN is intrinsically disordered (5, 6), it readily aggregates to oligomers, protofilaments, and fibrils (7, 8). αSN aggregation is extremely complex and depends on many different pathways and factors (9). The most toxic species, oligomers accumulate in the early stages of the fibril formation process and are thought to cause membrane destabilization (10), cytoskeletal changes (11, 12), mitochondrial dysfunction (11, 13, 14), and enhanced oxidative stress (11, 12, 15).

There has been an intense hunt for molecules that prevent αSN fibrillation and oligomerization and/or reduce the toxicity of preformed aggregated species. Inhibiting the interaction of oligomers with membranes, decreasing the production of reactive oxygen species (ROS) (16), and/or curbing rising cytoplasmic Ca^{2+} levels are very challenging.

This work was supported by Grant 982 from the Center for International Scientific Studies and Collaboration (CISSC) (to H. M. B., F. A., and D. M.), Grant 4005-00082 from the Independent Research Fund of Denmark, Technology and Production (to H. E., N. P. S., C. S., I. M. M., G. C., and D. E. O.), a grant to Rothamsted Research from the Biotechnology and Biological Sciences Research Council (BBSRC) of the UK (to C. L., A. T., and J. L. W.), and Tailoring Plant Metabolism Institute Strategic Programme Grant BB/E/C/000I0410 funded by the BBSRC (to J. W.). The authors declare that they have no conflicts of interest with the contents of this article.
This article contains Tables S1–S3 and Figs. S1–S14.
[1] To whom correspondence may be addressed. E-mail: beigi@inano.au.dk.
[2] Present address: Dept. of Chemistry, Center for Theoretical Biological Physics, Rice University, Houston, TX 77005.
[3] To whom correspondence may be addressed. E-mail: morshedi@nigeb.ac.ir.
[4] To whom correspondence may be addressed. Tel.: 45-20725238; E-mail: dao@inano.au.dk.

[5] The abbreviations used are: PD, Parkinson's disease; αSN, α-synuclein; ROS, reactive oxygen species; SEC-MALS, size-exclusion chromatography–multiangle light scattering; MTT, 3-(4,5-dimethylthiazol-2-yl)-2,5-diphenyltetrazolium bromide; LDH, lactate dehydrogenase; UHPLC, ultrahigh performance liquid chromatography; DOPG, 1,2-dioleoyl-*sn*-3-phosphatidylglycerol; T, Tarom varieties; DMPG, 1,2-dimyristoyl-*sn*-glycero-3-phospho-(1′-rac-glycerol); TEM, transmission electron microscopy; DCFH-DA, 2′,7′-dichlorodihydrofluorescein diacetate; ThT, thioflavin T.

The olive tree (*Olea europaea*) is the major source of fat in the Mediterranean diet (17), characterized by high plant food content. The Mediterranean diet is rich in antioxidants found in olive or other plant foods that may help lower oxidative stress in brain aging by affecting the expression of genes related to oxidative stress and markers of lipid oxidation (18) as well as protecting cells against oxidative damage (19). Olive phenolic compounds protect against a number of chronic degenerative conditions and are also implicated in the antioxidant, analgesic, anti-inflammatory, antitumor, antiviral properties of the olive (20, 21). They also inhibit self-assembly of Aβ42, Tau, and αSN (22–24) into amyloids and toxic aggregates, possibly by preventing $\pi-\pi$ and/or hydrophobic interactions (25, 26) and by redirecting these proteins into alternative nontoxic aggregates. Palazzi *et al.* (27) showed that oleuropein aglycone keeps αSN unfolded, rescues cells from oligomer toxicity, probes disaggregation of αSN aggregation, and prevents αSN binding to membranes. It has also been shown that olive biophenols could reduce the enzyme-induced toxicity associated with the oxidative stress involved in the progression of Alzheimer's disease (28). Among these compounds, some such as phenolic acids and flavonoids are found in many fruits. However, the secoiridoids are present exclusively in plants belonging to the family of Olearaceae, which includes *O. europaea* L. (29). Secoiridoids include oleuropein (responsible for the bitter taste of olive fruits) and structurally related glucosides. The content of the polyphenols of olive fruit depends on the olive cultivar and the fruit ripening stage (30, 31). There are hundreds of olive varieties, classified based on their origin. Selection and promotion of beneficial polyphenol-rich olive varieties for long-term use may help combat PD at the population level.

Although we do not claim that overall effects of a Mediterranean diet can be reproduced in their entirety by one or a few specific compounds, it is of basic interest to compare different olive varieties and establish causal relationships explaining their different effects. Comparison of complex mixtures such as different olive varieties under the controlled conditions has the potential to provide simple and straightforward information about the most important contributors to anti-aggregative and thus potentially anti-PD effects. Accordingly, we systematically screened extracts from different olive varieties for their ability to inhibit αSN fibrillation and formation of toxic aggregates. The assays monitored (*a*) kinetics, extent, and end products of αSN fibrillation; (*b*) formation of toxic oligomers, disaggregation of preformed fibrils, induced changes in αSN through interaction with anionic vesicles, and vesicle permeabilization induced by oligomers in the presence and absence of the extracts, and (*c*) toxicity of both extracts and αSN aggregates formed in the presence of extracts. The assays identified the extract, which most efficiently inhibited αSN fibrillation. The best extract in inhibiting αSN fibrillation was fractionated and the compounds present in these fractions were identified by LC-MS analysis.

Results

Selection of olive fruits and preparation of the extracts

Methanolic extracts were obtained from fruits of different olive varieties (Table S1). Of these, the Mediterranean varieties Koroneiki, Arbequina, and Picual are the world's most prestigious varieties for super high density cultivation systems with excellent oil quality characteristics (32). Zard, Mari, and Rowghani are three prevailing varieties in Iran primarily used in olive oil production. The third group consisted of nine Iranian Tarom olive varieties (T10, T15, T16, T17, T18, T20, T22, T23, and T24).

Screening against αSN aggregation based on ThT screening assays

We first screened extracts for their ability to inhibit αSN aggregation using different ThT-based plate reader assays. αSN aggregation in PBS buffer was accelerated by shaking in the presence of glass beads (31).

In the fibrillation assay, all 15 extracts showed an aggregation–inhibitory effect at 0.025 and 0.3 mg/ml by reducing the end point ThT fluorescence level, although to different extents. At 0.3 mg/ml, 7 of the 15 extracts (T10, T17, T20, T23, T24, Rowghani, and Koroneiki, in blue in supporting Fig. S1, *A* and *B*) reduced end point ThT levels to 1–15% of the control in the absence of extracts. The following experiments described in this paper focus only on these most effective 7 extracts. Dose-response curves were then recorded (Fig. 1*A*) and the normalized maximum ThT intensity (Fig. 1*B*) was used to obtain IC_{50} values (Equation 1) of the 7 top-ranked extracts (Fig. 1*C*). Here, the Koroneiki extract emerged as the best inhibitor. The Finke-Watzky model (Equation 2) was fitted to the ThT kinetic data (kinetic data are summarized in Fig. 1, *D–F*) to obtain two central parameters, namely $t_{½}$ (the time required to produce half the total product) and ν (the rate of growth at $t_{½}$), from which the lag or nucleation time t_N could be calculated. The extracts reduced the level of fibrillation to different extents. All extracts except T24 produced a concentration-dependent reduction of ν and increase of $t_{½}$ compared with control.

Far-UV CD spectroscopy (CD), SDS-PAGE, and transmission electron microscopy (TEM) images validated ThT data by providing independent measurements of the extent of fibrillation and the structure of the final aggregates. Remarkably, several of the extracts maintained αSN in a largely unfolded conformation (Fig. 2, *A–C*), particularly at 0.3 mg/ml of extract. The normalized β-sheet content (%) of αSN is shown in Fig. 2*D*. The Koroneiki extract was particularly effective at retaining the unfolded conformation of αSN, and its preeminence compared with the other extracts became more obvious as the extract concentration was reduced to 0.15 and 0.1 mg/ml. T17, T20, T23, and T24 were least efficient in this regard, in good agreement with the ranking from the fibrillation assay.

SDS-PAGE was used to analyze the amount of soluble αSN in the supernatant after centrifugation. The 7 extracts significantly increased the amount of monomer left in the solution after 24 h incubation (Fig. 2*E* and Fig. S2). Low, but detectable amounts of dimers and larger aggregates are also visible in the presence of some of the extracts. For additional confirmation, the supernatants of the incubated samples of αSN in the absence and presence of 0.3 mg/ml of Koroneiki were run on a gel filtration column. As shown in Fig. 2*F*, Koroneiki significantly increased the amount of monomer left in the solution after a 24-h incubation. Two populations of oligomers were also detectable after gel filtration of samples with Koroneiki.

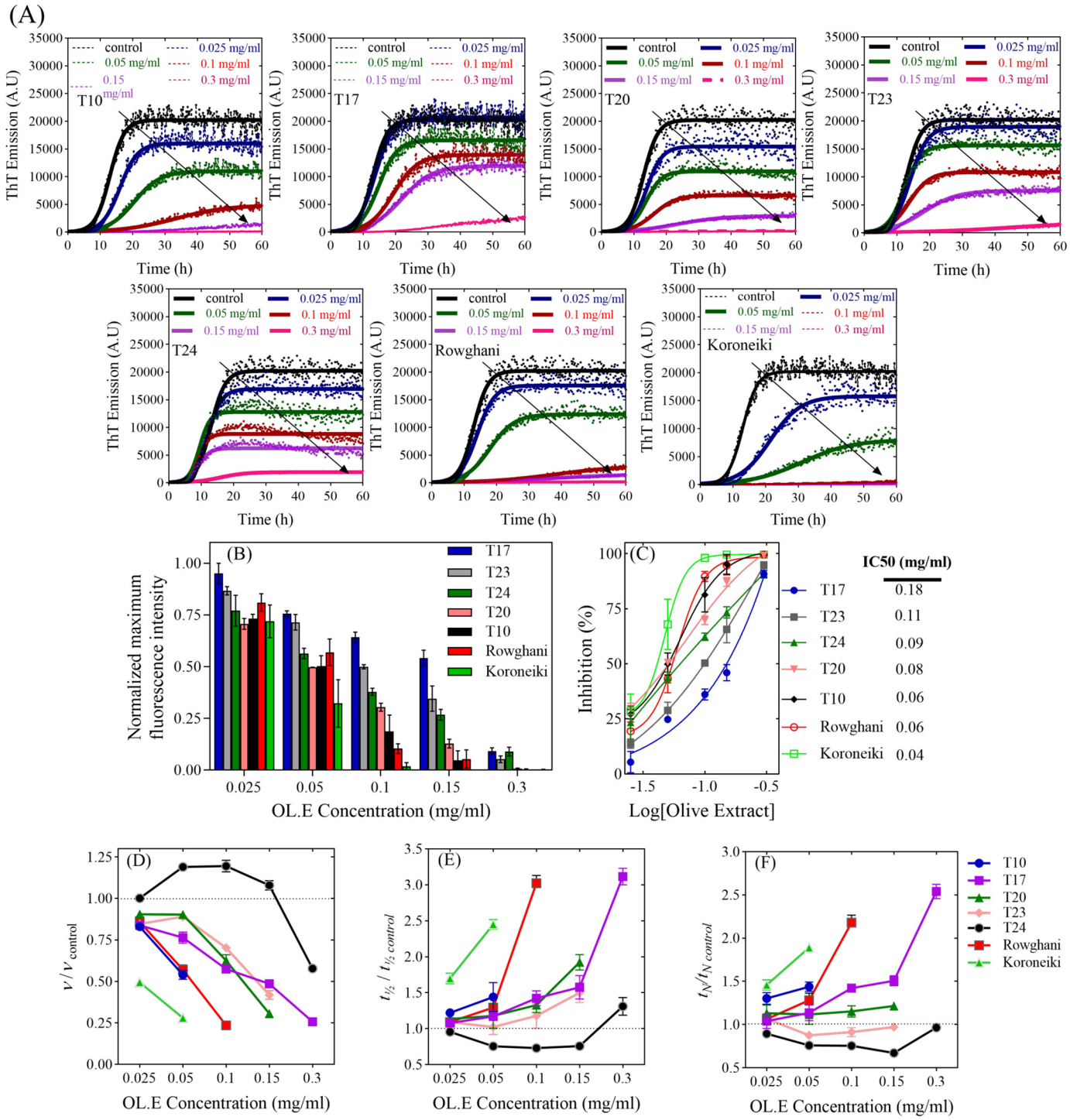

Figure 1. The effect of the extracts on αSN fibrillation. *A*, the effect of 0–0.3 mg/ml of the olive extracts on the kinetics of αSN fibrillation at 5 different concentrations monitored by ThT fluorescence. *Joined lines* show the Finke-Watzky model fitted to the experimental data. *B*, the effect of the selected extracts (7 of 15 extracts) at different concentrations (0.025, 0.05, 0.1, 0.15, and 0.3 mg/ml) on the maximum ThT fluorescence intensity. *C*, ThT end point levels are converted to % inhibition and fitted to Equation 1 to calculate the IC_{50} of the extracts. *D–F*, kinetic parameters for αSN fibrillation as a function of various concentrations of the extracts relative to the values in the absence of the extracts (*D*, relative growth rate ($\nu/\nu_{control}$); *E*, relative half-time ($t_{1/2}/t_{1/2,\,control}$), and *F*, relative lag time ($t_N/t_{N,\,control}$)).

The effect of 0.3 mg/ml of extract on the morphology of end point αSN aggregates was analyzed by TEM (Fig. 2*G* and associated table). Although the limited quantitative output from these TEM analyses preclude detailed comparison with ThT parameters such as lag time and growth rates, there is good qualitative agreement: Koroneiki and Rowghani extract completely suppress fibril formation and only oligomers are detectable, just as they very efficiently suppress ThT signals. The other extracts reduce fibril formation to a somewhat smaller extent, but still lead to significant reductions compared with the control, consistent with their overall reduction of ThT signal.

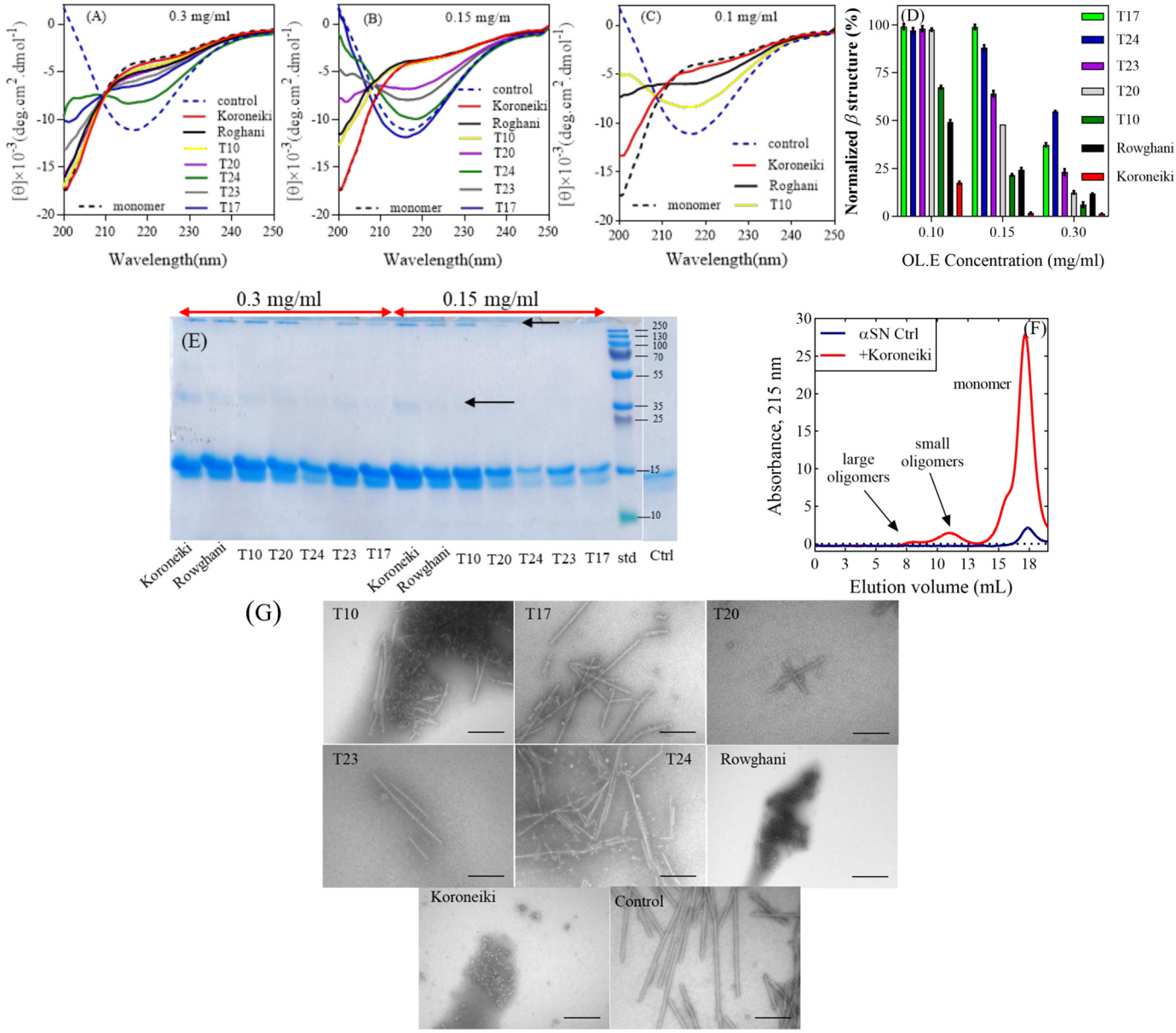

Sample	Average Length of fibrils (μm)	Number of fibrils measured	Comments
αSN+T10	0.37±0.087	10	small unstructured aggregates + few fibrils
αSN+T17	0.33±0.19	25	few fibrils with broad size distribution
αSN+T20	0.2±0.053	10	very few small fibrils
αSN+T23	0.32±0.081	10	very few small fibrils
αSN+T24	0.5±0.12	28	few fibrils with broad size distribution
αSN+Rowghani	None detected	0	small aggregates without any fibrils
αSN+Koroneiki	None detected	0	small aggregates without any fibrils
αSN Control	0.68±0.092	40	large homogeneous fibrils everywhere on the grid

Figure 2. Far-UV CD spectra of αSN incubated alone (control) and in the presence of (*A*) 0.3 mg/ml, (*B*) 0.15 mg/ml, and (*C*) 0.1 mg/ml of the 7 selected extracts after 24 h. *D*, normalized β structure (%) of αSN incubated in the presence of the 7 selected extracts. *E*, SDS-PAGE analysis of the supernatants of the incubated samples of αSN in the absence and presence of 0.15 and 0.3 mg/ml of the best extracts in inhibiting αSN fibrillation. Monomeric αSN has a molecular mass of 14.5 kDa. *Arrows* highlight dimers (≈35 kDa) and oligomers (>250 kDa). *F*, the SEC-profile of the supernatants of the samples of αSN incubated for 24 h with or without 0.15 mg/ml of Koroneiki extract. *G*, EM of αSN after 24 h incubation in the absence (control) and presence of 0.3 mg/ml of the 7 selected olive fruit extracts. *Scale bar*, 200 nm. The size and distribution of the fibrils in each sample are summarized in the table below *G*. The length of fibrils were obtained in three TEM images for each sample and averaged.

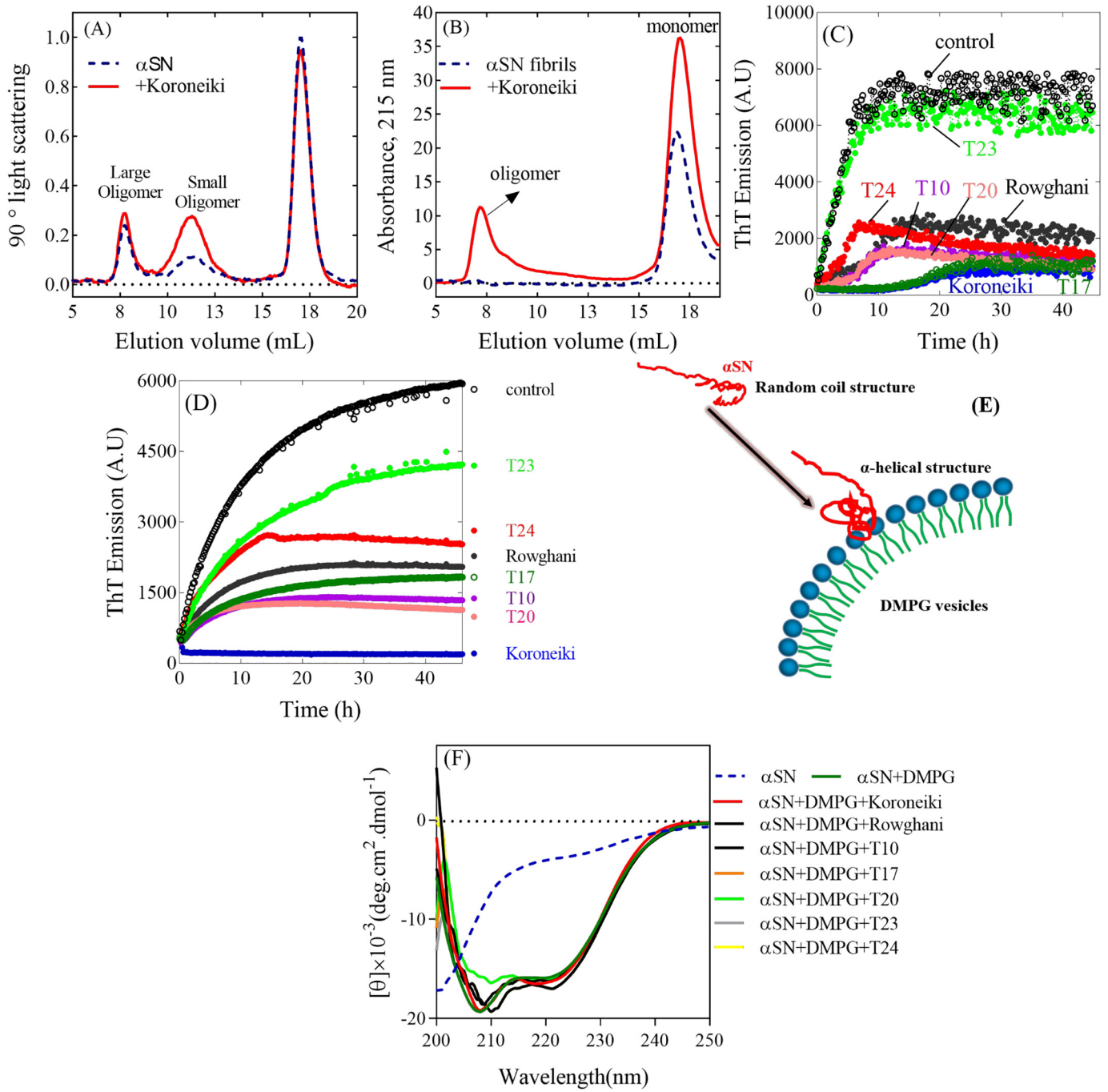

Figure 3. The SEC-profile of the supernatants of the (*A*) samples of αSN incubated for 1 h and (*B*) preformed αSN fibrils preincubated overnight with or without 0.15 mg/ml of Koroneiki extract. The effect of the extracts (0.15 mg/ml) on the seeding of αSN aggregation under shaking (*C*) and nonshaking (*D*) conditions. *E*, schematic representation of the α-helix structure induced in αSN by DMPG vesicles. *F*, the effect of the extracts (0.15 mg/ml) on the interaction of monomer (14 μM) and DMPG vesicles (0.2 mg/ml).

Olive fruit extracts induce formation of different oligomers

To study the effect of the extracts on the formation of soluble aggregates, we prepared oligomeric species of αSN in the presence and absence of 0.15 mg/ml of extracts. Although fibrillation of αSN is a slow process with lag times of 10–20 h depending on protein concentration (33), oligomer formation occurs over a few (<5) hours. We have previously shown that during the oligomerization (900 rpm, 37 °C), αSN forms two populations of oligomers, largely elongated oligomers and small spherical oligomers, which increase slowly over time (7, 34). The small oligomers, estimated to contain ~30 monomers, form a compact prolate ellipsoid core with a number of flexible chains protruding from the surface into the solution, whereas the larger oligomers are concatemers of the smaller ones (34).

We used SEC-MALS (Fig. 3*A* for Koroneiki and Fig. S3 for the others), a technique in which species are separated according to hydrodynamic radius on a SEC column, after which the concentration of the species are obtained from the peak area under the MALS peaks. We did not estimate oligomer concentration based on absorption at 280 or 215 nm, because extract

binding to the oligomers could affect absorption. Instead we used MALS data to allow more direct comparison of oligomer yields. This ranked the amount of large oligomers formed in the presence of the extracts in the following order: T23 > Rowghani > T10 ≈ T17 ≈ T24 > Koroneiki > T20, which differed significantly from that of the small oligomers (Koroneiki > T10 > T23 ≈ Rowghani ≈ T10 ≈ T17 ≈ T 24). In all cases, the level of monomers was relatively unchanged, indicating that most αSN remained unaggregated.

Olive fruit extracts disaggregate preformed fibrils

We next used gel filtration to address whether overnight incubation with extracts could disaggregate existing αSN fibrils. We monitored this process by absorption at 215 nm, because we were mainly concerned with the appearance of soluble αSN. Addition of olive extracts led to an increase in the monomer peak, as well as the formation of soluble oligomers (eluting at 5–10 ml), particularly in the presence of 0.15 mg/ml of Koroneiki extract (Fig. 3*B*). Additional peaks eluting after the αSN monomer peak are C-terminal fragments of αSN formed by chemical cleavage after long-term incubation.[6] Thus existing fibrils could be disaggregated by Koroneiki extract at concentrations that also completely inhibited aggregation. The other extracts had less dramatic effects (Fig. S4), although T17 and T20 extracts in particular increased the monomer population to some extent.

Olive fruit extracts inhibit fibril elongation

To determine whether or not the extracts could affect elongation of existing fibrils, short fibrillar seeds (5%) were added to monomeric αSN. This bypasses the nucleation step and allows us to study the elongation of existing fibrils. Koroneiki extract was the most effective inhibitor in both shaking and nonshaking assays, leading to a very extended lag phase of fibrillation (≈10 h) under shaking conditions and completely suppressing fibril growth over a 45-h observation period in the absence of shaking (Fig. 3, *C* and *D*). The other extracts reduced elongation rates to different extents. T23 extract performed most poorly in both assays, whereas T17, T10, and T20 extracts performed quiet well although not as well as Koroneiki extract. Thus, Koroneiki extract was the best inhibitor of both nucleation and fibril elongation.

Olive fruit extracts do not inhibit the change in αSN structure induced by vesicles

Interaction with anionic phospholipid vesicles induces a major increase in α-helical structure in αSN (35) (Fig. 3*E*). Compounds such as squalamine can displace αSN from lipid membranes and decrease the α-helical content of αSN (36). However, even at the high concentration of 0.15 mg/ml, none of the extracts prevented monomeric αSN from forming an α-helical structure in the presence of anionic vesicles of DMPG (Fig. 3*F*). Consistent with this, the Koroneiki extract failed to show any effect at other concentrations (0.025–0.3 mg/ml, data not shown).

[6] C. Sahin, T. J. D. Jørgensen, and D. E. Otzen, unpublished results.

Olive fruit extracts are nontoxic, show antioxidant activity, and decrease the level of ROS in OLN-93 cells

We evaluated the antioxidant activity of the olive extracts at 0.02–0.12 mg/ml using the DPPH$^{\bullet}$ assay. All extracts showed similar dose-response levels in this assay (Fig. S5*A*). Furthermore, none of the extracts showed significant toxicity on their own toward OLN-93 and SH-SY5Y cells according to the 3-(4,5-dimethylthiazol-2-yl)-2,5-diphenyltetrazolium bromide (MTT) assay (Fig. S5, *B* and *E*).

We used DCFH-DA to evaluate extract effects on ROS production in OLN-93 cells. All extracts except T24 decreased free radical formation (Fig. S5*C*). Furthermore, all extracts neutralized the deleterious effect of 100 μM H_2O_2 (Fig. S5*D*) to the same concentration-independent extent.

Olive fruit extracts induce formation of less toxic aggregates and reduce the cytotoxicity of oligomers to the SH-SY5Y cells

We evaluated the membrane permeabilization and cytotoxicity of aggregates formed during different stages of αSN fibrillation with and without extracts (Fig. 4*A*). Without extracts, the ability of aggregates to release calcein decreased as the aggregates aged over 24 h (Fig. 4*B*); several of the extracts, particularly Koroneiki, accelerated this decline. This suggests that aggregates formed in the presence of the extracts interact less with the membranes.

In the MTT cell viability assay with OLN-93 and SH-SY5Y cells, aggregates formed in the presence of the extracts showed less cytotoxicity than the extract-free αSN control samples (Fig. 4, *C* and *D*). The aggregates were more toxic to OLN-93 cells (Fig. 4*C*) than to SH-SY5Y cells (Fig. 4*D*). Whereas all extracts significantly enhanced viability of OLN-93 cells at the early stages (4, 8, and 12 h), at 24 h this effect is just significant for T17, Rowghani, and Koroneiki extracts. However, for SH-SY5Y cells, this enhancement effect is retained for all extracts and all incubation times (Fig. 4*D*). A difference in response by different cell lines is not without precedent; we have also recently reported that SH-SY5Y and PC-12 cells (another neuronal cell line) differ in their sensitivity to αSN aggregates (37).

We needed to rule out that the reduced toxicity of aggregates formed in the presence of the extracts could be caused by a general effect of the extracts on the cells. Therefore, we treated SH-SY5Y cells with Koroneiki extract, incubated the cells for 2 h, removed the solution, and washed the cells with PBS. Subsequently we added αSN aggregates both to extract-treated and untreated cells. We found no significant difference in aggregate toxicity on the two cell types (data not shown), ruling out a general extract effect.

Mitochondrial disruption induced by the aggregates was evaluated by the release of lactate dehydrogenase (LDH) (Fig. 4*E*). The aggregates formed without the extracts increased LDH release by 60–72% compared with control. However, LDH release was reduced significantly in cells treated with aggregates formed in the presence of the extracts. This is consistent with reduced cellular toxicity and confirmed that extracts reduce the toxicity of aggregates in the cell-based assays.

In the next step, the membrane permeabilization assay (Fig. 5*A*) was carried out to see if Koroneiki extract can decrease the

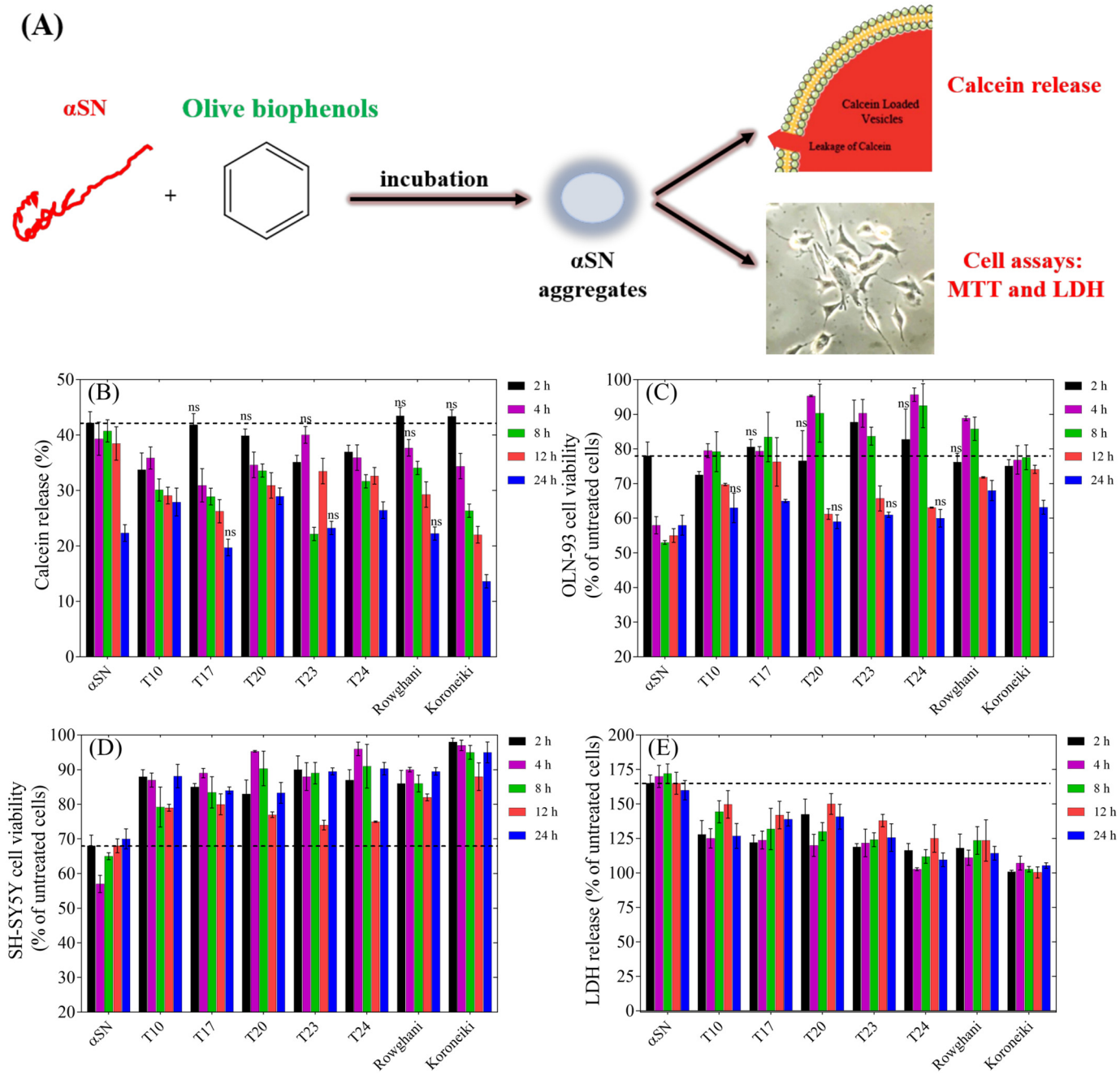

Figure 4. *A*, schematic representation of the effect of olive variety extracts on the membrane permeabilization and cytotoxicity of αSN aggregates. *B*, calcein release from DOPG vesicles after 20 min incubation with αSN aggregates formed alone and in the presence of the best extracts (0.3 mg/ml) over different times (0–24 h). Viability of OLN-93 (*C*) and SH-SY5Y (*D*) cells after 2–24 h incubation with αSN aggregates formed alone and in the presence of the best extracts (0.3 mg/ml) over different times (0–24 h). *E*, cytotoxicity of αSN aggregates to SH-SY5Y cells was assayed by LDH release. LDH signals were normalized to untreated cells. For all assays, values represent mean ± S.D. and the differences between the groups and αSN control are significant ($p < 0.05$) unless marked *ns*.

membrane-disrupting ability of αSN oligomers, which permeabilize the membrane (and by inference induce toxicity in cells). Fig. 5*B* shows that Koroneiki extract only leads to an insignificant reduction in oligomer-induced permeabilization of anionic phospholipids in a calcein release assay. The Koroneiki extract itself does not lead to any calcein release and loss of vesicle integrity (data not shown).

We finally tested the Koroneiki extract for its effect on oligomer toxicity in a cellular context (Fig. 5*C*). Purified oligomers decreased viability by 28% on their own but only by 15% in the presence of 0.15 mg/ml of Koroneiki extract. Thus, Koroneiki extract not only led to formation of less toxic and less cell-permeabilizing oligomers (Fig. 4, *B–D*), but also protected SH-SY5Y cells against preformed toxic oligomers (Fig. 5*C*). Koroneiki extract at 0.015 mg/ml did not significantly reduce the toxicity of oligomers (data not shown).

The chemical composition of different extracts

HPLC analysis of the most effective extracts revealed the same qualitative but different quantitative phenolic composi-

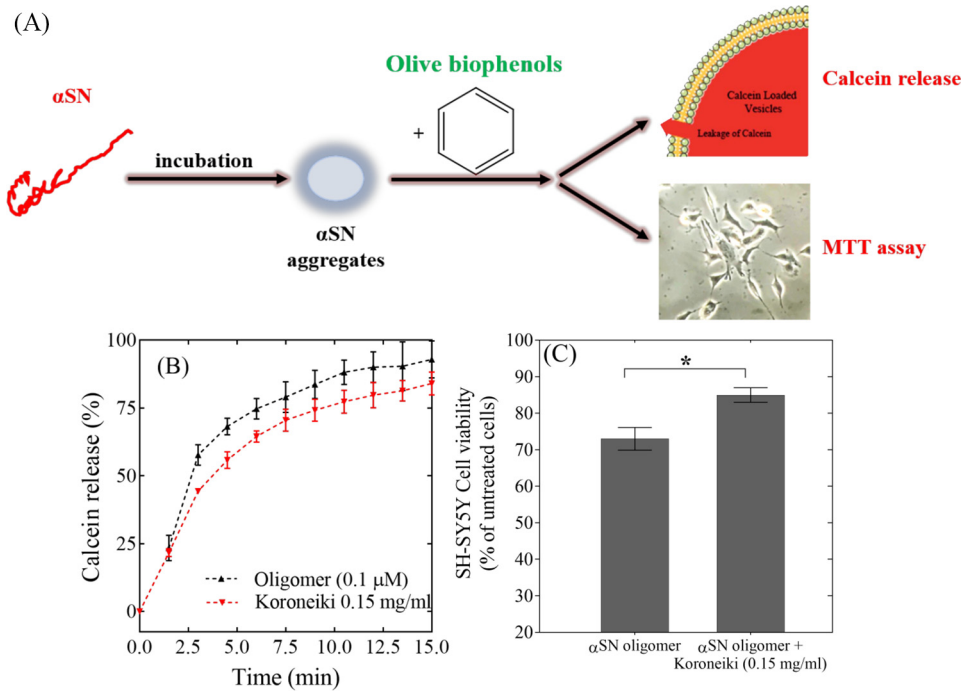

Figure 5. *A,* schematic representation of the effect of Koroneiki extract fractions on the membrane permeabilization and cytotoxicity of αSN aggregates. *B,* calcein release from DOPG vesicles induced by oligomers (0.1 μM) either alone or in the presence of Koroneiki (0.2 mg/ml). The Koroneiki extract is used at the highest concentration at which quenching of fluorescence does not happen. *C,* viability of SH-SY5Y cells incubated with αSN oligomers with or without co-incubation with Koroneiki (0.15 mg/ml).

tion for major components (Fig. S6). For more detailed studies, the Koroneiki extract was fractionated by UHPLC (Fig. S7), after which the inhibitory effect of the fractions was studied and the best fractions in inhibiting αSN fibrillation and reducing toxicity of αSN oligomers were analyzed on LC-MS to identify the compounds involved.

Identification of the most effective fractions

In the first step, the effect of fractions of the Koroneiki extract on αSN fibrillation was studied at two different concentrations. These are designated L and H (low and high). L and H fractions are obtained from 1 and 3 mg/ml of Koroneiki extract, respectively, which implies that the concentration of the factions in the fibrillation assays are much less than 1 and 3 mg/ml. The most effective fractions (5, 6, and 17–26) are indicated in *red* in Fig. S8, *A* and *B*, whereas the time profiles of fibrillation are shown in Fig. S9. CD and TEM images were used to confirm the ThT data and better understand their effect on αSN fibrillation. CD data (Fig. 6, *A* and *B*) show that the most effective fractions maintained the unfolded secondary structure of αSN. The effect of the fractions at 3 mg/ml on the morphology of end point αSN aggregates was analyzed by TEM (Fig. S10). In the presence of the fractions, either only oligomers (f5, 18, 21, 23, and 25) or both short fibrils and oligomers (f6, 17, 19, 20, 24, and 26) were detectable. In contrast, the control sample without the Koroneiki extract fractions only showed long straight fibrils.

To determine whether or not the fractions affect elongation of existing fibrils, we incubated monomeric αSN with 5% αSN seeds. Fractions 19–23 were the best inhibitors of secondary nucleation (Fig. 6*C*). The other fractions did not completely inhibit seeded fibrillation but instead decreased the rate of elongation, increasing the time it took for the ThT fluorescence to reach a plateau level.

The effect of the top 12 fractions identified in the ThT assay on the level of small and large oligomers and their ability to disaggregate existing fibrils of αSN was also studied. Fractions 6, 18, and 21–23 led to the formation of more small oligomers (Fig. S11*A*). Disaggregation of αSN fibrils by Koroneiki fractions also led to the formation of soluble oligomers (Fig. S11*B*) and fractions 5, 20, and 24–26 were the most effective.

Identification of the antioxidant activity and toxicity of different Koroneiki extract fractions

We evaluated the antioxidant activity of the Koroneiki fractions using the DPPH• assay. Fractions with the most inhibitory effect (f5, 6, and 17–26) showed more inhibition (%) and scavenging ability (Fig. S12*A*). When these fractions were incubated with OLN-93 and SH-SY5Y cells, they showed no significant toxicity at 1 and 2 mg/ml (Fig. S12, *B* and *C*); however, fractions 19, 21, 23, and 25 were slightly toxic to OLN-93 cells at the highest concentration tested (3 mg/ml).

The most effective fractions induce the formation of less toxic aggregates

The same toxicity assay as for whole extracts was used to evaluate the toxicity of formed aggregates during the fibrillation process either in the presence or absence of the Koroneiki fractions. The calcein release assay showed a reduction in the interaction of the aggregates formed up to 24 h in the presence of fractions with the membranes compared with the control samples (Fig. 6*D*). In the cell assay on both OLN-93 and SH-SY5Y cells, the toxicity of control aggregates formed up to

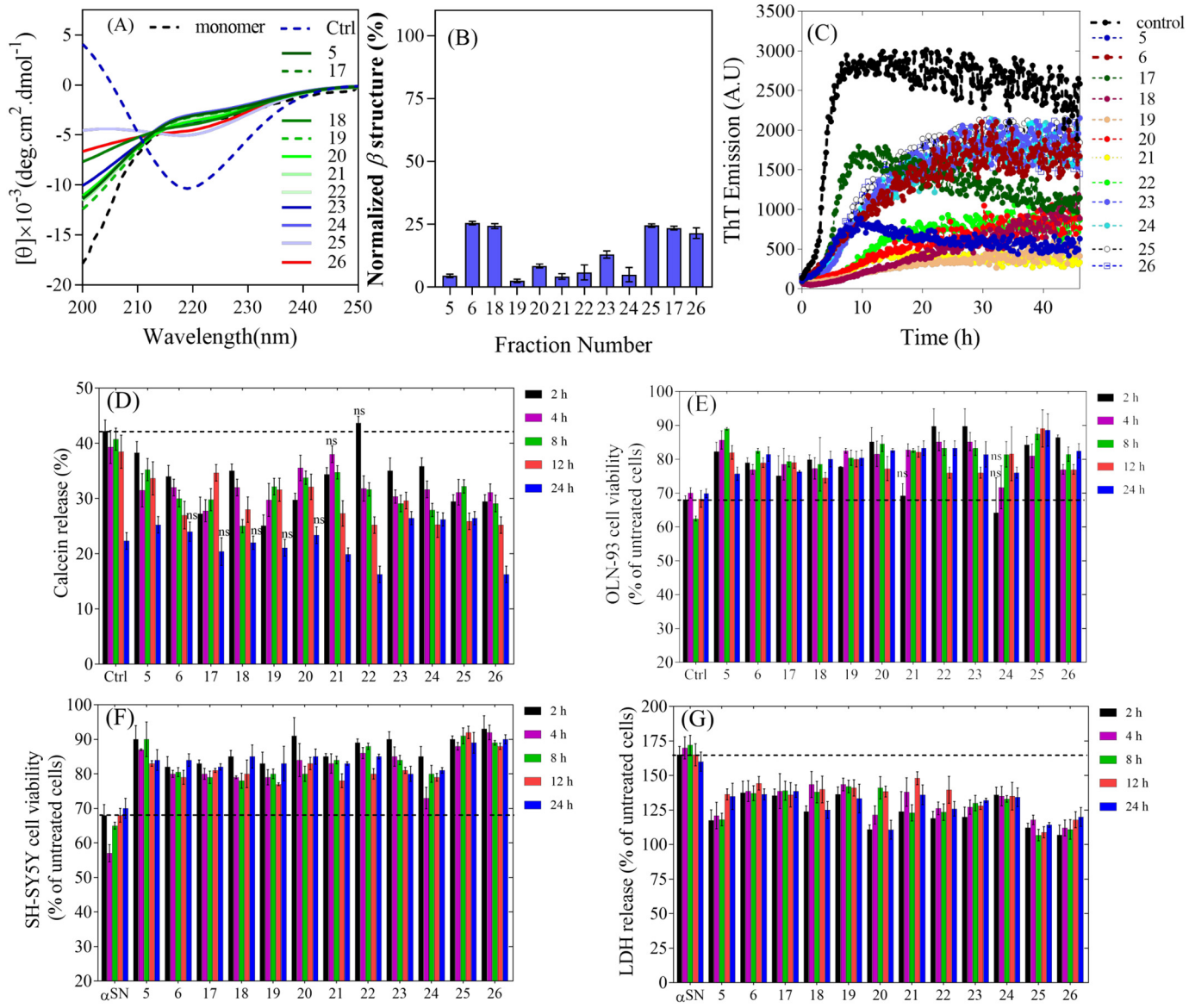

Figure 6. *A*, far-UV CD spectra of αSN incubated alone (control) and in the presence of 3 mg/ml of Koroneiki extract fractions. *B*, normalized β structure (%) of αSN incubated in the presence of Koroneiki extract fractions. *C*, the effect of the Koroneiki extract fractions (1.5 mg/ml) on the seeding of αSN aggregation under shaking conditions. *D*, calcein release from DOPG vesicles after 20 min incubation with αSN aggregates formed alone and in the presence of Koroneiki extract fractions (3 mg/ml) over different times (0–24 h). Viability of OLN-93 (*E*) and SH-SY5Y (*F*) cells after 24 h incubation with αSN aggregates were formed alone and in the presence of Koroneiki extract fractions (3 mg/ml) over different times (0–24 h). *G*, cytotoxicity of αSN aggregates to SH-SY5Y cells was assayed by LDH release. LDH signals were normalized to untreated cells. For all assays, values represent mean ± S.D. and the differences between the groups and αSN control are significant ($p < 0.05$), unless indicated *ns*.

8 h increased and then decreased slightly. Aggregates formed in the presence of the Koroneiki fractions also generally showed an increase in cytotoxicity at early stages, but the levels of toxicity were reduced compared with control, in particular for fraction 25 (Fig. 6, *E* and *F*). Overall, the LDH assay in SH-SY5Y cells also confirmed these data (Fig. 6*G*).

Separation and identification of phenolic compounds in the most effective fractions

We used LC-MS analysis of the most effective Koroneiki fractions to separate and identify major components of these fractions. Identification of the compounds was done based on accurate mass measurements of the $[M\text{-}H]^-$ ion and their MS-MS fragmentation patterns as documented in the literature. The total ion current profiles of representative olive fractions are presented in Fig. S13. Data obtained from high resolution MS analysis of the fractions are summarized in Table S2. The major compounds in each fraction are listed in Table S3 and indicated on the total ion current profiles of individual fractions (Fig. S13). It is clear that the single largest family of compounds consists of oleuropein and derivatives thereof. For additional insight, we tested individual compounds identified in the Koroneiki fractions, namely verbascoside, loganin, rutin, elenolic acid, 3-hydroxytyrosol, and oleuropein. The compounds effects on αSN fibrillation were tested through ThT-based kinetics, CD spectroscopy, and TEM imaging (Fig. 7). ThT data (Fig. 7*A*) show that verbascoside, elenolic acid, 3-hydroxytyrosol, and oleuropein completely inhibit fibrillation at

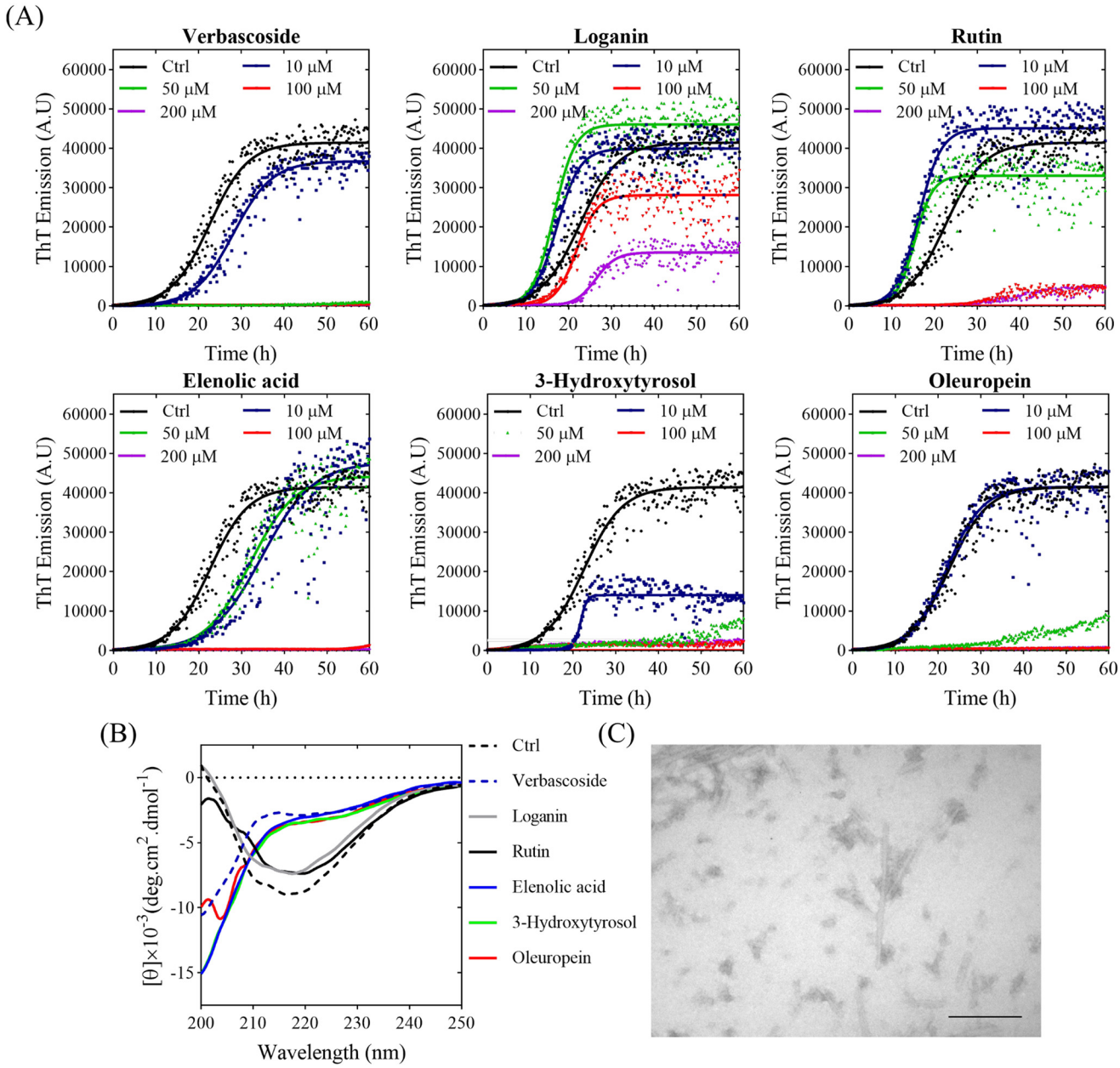

Figure 7. The effect of Koroneiki compounds on fibrillation of 1 mg/ml αSN. *A,* the kinetics of αSN fibrillation in the presence of 0–200 μM Koroneiki compounds, monitored by ThT fluorescence. *B*, far-UV CD spectra of αSN incubated alone (*Ctrl*) and in the presence of 200 μM Koroneiki compounds after 24 h. *C,* EM of αSN after 24 h incubation in the presence of 200 μM oleuropein. *Scale bar*, 200 nm.

50 (verbascoside) or 100 μM (all other compounds), comparable with the effect of (−)-epigallocatechin-3-gallate (38). The CD data (Fig. 7*B*) also show that these compounds keep αSN in its monomeric unfolded state better than other compounds. Finally, TEM images of αSN after incubation in the presence of oleuropein confirm the absence of fibrils (Fig. 7*C*).

Correlating the change in the chemical compositions of extracts with their inhibitory effect

We also analyzed extracts from developing fruits to correlate the change in the chemical composition of the extracts with their inhibitory effect. During the ripening process and fruit development, the phenolic content changes (31). Accordingly, we collected olive fruits at different ripening time and the effect of the extracts was tested on αSN fibrillation. The HPLC data and the effect of the extracts are shown at Fig. S14. Then the average values of the end ThT values of αSN aggregation in the presence of different amounts of olive extracts (the 9 top-ranked extracts as well as extracts of fruits collected at different ripening times) were combined with the HPLC data of the olive samples to analyze the effect of different compounds in the extracts. The "peakutils" Python package was used to identify peaks in the HPLC data. Finally, a correlation analysis was performed to determine which peaks have correlated amounts across all of the samples. This analysis confirmed that the compound eluting as oleuropein aglycone, which also shows the highest m-value as a measure of its anti-fibrillation potency, is of interest because the level of that compound was not well

Table 1
For each olive extract constituent, coefficient of determination (R^2), the slope of the optimal linear fit (m-value), and Spearman's rank correlation coefficient for each compound

Peak elution time	Compound	*R*-squared[a]	m-value[b]	Spearman *R*[c]
35.5	Oleuropein	0.29	−11.76	−0.73
28.5	Verbascoside	0.39	−24.69	−0.71
50.3	Oleuropein aglycon	0.48	−88.31	−0.76
40.0	Hydroxy oleuropein aglycone	0.24	−24.13	−0.72

[a] Coefficient of determination: measures the goodness of fit assuming a linear model.
[b] The slope of the optimal linear fit (the m-value): measures the potency with larger (negative) slopes corresponding to more potent inhibition.
[c] Spearman's rank correlation coefficient: measures how monotonically related the two quantities are without making an assumption about the functional form of the relationship.

correlated with other compounds and was therefore more likely to be responsible for the difference in inhibition across the extracts (Table 1). Comparison of HPLC chromatograms of extracts of fruits picked at different ripening time with their inhibitory effect (Fig. S14) revealed that the extracts with a higher level of oleuropein aglycone had more inhibitory potency; in contrast, the levels of other compounds were lower compared with the less effective extracts.

Discussion

In PD, αSN aggregation initiates a cascade of molecular events leading to neuronal death. As a consequence, the identification of small molecules able to interfere *in vivo* with aggregation of αSN is a vital strategy against PD. Here we address three questions to identify olive oils with maximal anti-aggregative effects. 1) What is the mechanism behind the inhibiting effect of beneficial polyphenols? 2) Can these polyphenols lead to the formation of less toxic aggregates? 3) How do the level of beneficial polyphenols change with time?

The best extracts in inhibiting αSN fibrillation inhibit both nucleation and elongation of αSN

A summary of the efficacy of the olive extracts and the Koroneiki extract fractions in different assays is shown in Tables 2 and 3, respectively. We scored each assay between 0 and 1 and then determined the final ranking. We classified extracts of 7 of 15 different olive varieties according to their efficacy in inhibiting distinct steps of αSN aggregation (nucleation and elongation). Although the ranking differed slightly in different assays, all assays emphasized the remarkable inhibitory effect of the Koroneiki extract as the best inhibitor of both nucleation and elongation. Koroneiki, "the queen of olives," is a variety with particularly good oil quality characteristics, making it the main olive oil produced in Greece (39). Koroneiki and T20 varieties were most effective in the disaggregation assay, whereas Rowghani, which had performed well in the other assays, performed poorly here. These extracts may interact with the hydrophobic residues of β-sheet and cause disaggregation of amyloid fibrils. The different rankings indicate that these extracts are likely to bind both nuclei and fibril surfaces and ends, but to different extents.

The best extracts in inhibiting αSN fibrillation favor less toxic oligomeric species

Inhibition of aggregation could bypass the formation of toxic prefibrillar aggregates and direct αSN toward less toxic aggregates. SEC analysis and SDS-PAGE were used to analyze the aggregates that form in the presence of the extracts. Interestingly, Koroneiki extract, which was the best inhibitor, also ranked top in the formation of small oligomers and only led to a low production of large oligomers, whereas the T23 extract, which performed poorly in all other assays, strongly favored large oligomers. The SDS-PAGE results also indicate that the great majority of the αSN remains monomeric and the TEM images showed a reduction in longer fibrils at the fibrillation assay end point in the presence of the extracts. We therefore conclude that the most promising extracts inhibit αSN amyloidogenesis by retaining αSN in the monomeric state, and incorporating minor amounts of αSN monomers into highly stable oligomers that are noncytotoxic and off-pathway to fibrillogenesis (16), thereby inhibiting the subsequent growth phase (Fig. 8).

This change in the aggregation process also reduces cytotoxicity. Co-incubation of monomeric αSN with Koroneiki extracts lead to the formation of aggregates that, particularly after longer incubation, permeabilized membranes significantly less than the control aggregates and were less toxic to OLN-93 and particularly to SH-SY5Y cells. Some compounds are known to inhibit the membrane interactions of preformed αSN oligomers (16, 40). This is not the case for Koroneiki extract, which did not reduce the interaction of αSN monomers or preformed αSN oligomers with membranes, so the reduction in cytotoxicity of preformed αSN oligomers must derive from another as yet unknown mechanism, rather than by reducing membrane interactions.

αSN is susceptible to oxidative stress, which in turn favors its aggregation (41), and oligomeric species formed in the aggregation process can induce oxidative stress (42). Therefore, extracts and compounds that inhibited both αSN aggregation and ROS production would be promising. The extracts themselves showed no toxicity to OLN-93 and SHSY5Y cells. All extracts showed significant antioxidant activity and neutralized the deleterious effect of H_2O_2 on cells with different potency. This protective effect other than the scavenging of free radicals could be due to the effect at the molecular level of the cells such as activation of signaling cascades and regulation of calcium ion homeostasis (43).

Oleuropein aglycone, hydroxy oleuropein aglycone, and oleuropein are mainly responsible for the difference in inhibition across the extracts

An understanding of the molecular mechanism of olive extract-induced inhibition is complicated by the polyphenolic complexity as evidenced by LC-MS. In addition to polyphenols, such as flavonoids found in many fruits, oleuropein and other glucosides structurally related to this compounds are present exclusively in olive plants. Using the same assays as used for ranking the extracts, the inhibitory effect of fractions of the Koroneiki extract was tested on αSN fibrillation. Phenolic com-

Table 2
Ranking of the top 7 olive variety extracts in different assays

Assay	T10	T17	T20	T23	T24	Rowghani	Koroneiki	Ref.
Inhibiting aggregation[a]	++++	++	+++	++	+++	++++	++++	Fig. 1
Inhibiting secondary nucleation[b]	++++	+++	++++	++	+++	+++	++++	Fig. 3
Formation of small oligomers[c]	+++	+++	++	++	++	++	++++	Fig. 3
Formation of large oligomers[d]	++	++	+	++++	++	+++	+	Fig. 3
Inducing formation of less toxic aggregates to SH-SY5Y cells during fibrillation[e]	++++	++++	+++	+++	+++	++++	++++	Fig. 4

[a] At 0.1 mg/ml of the olive extracts, + denotes 0–25% inhibition, ++ 25–50% inhibition, +++ 50–75% inhibition, and ++++ 75–100% inhibition.
[b] At 0.15 mg/ml of the olive extracts, + denotes 0–25% inhibition, ++ 25–50% inhibition, +++ 50–75% inhibition, and ++++ 75–100% inhibition.
[c] At 0.15 mg/ml of the olive extracts, Min (small oligomer) = A, Max (small oligomer) = B, x = $(A-B)/4$. + denotes $A <$ (small oligomer) $< A + x$, ++ denotes $A + x <$ (small oligomer) $< A + 2x$, +++ denotes $A + 2x <$ (small oligomer) $< A + 3x$, and ++++ denotes $A + 3x <$ (small oligomer) $< B$.
[d] The same formula for ranking as in footnote c, this time using the large oligomers.
[e] Average of toxicity of aggregates formed over different time ranges compared to control.

Table 3
Ranking of the fractions in different assays

Assay	5	6	17	18	19	20	21	22	23	24	25	26	Ref.
Inhibiting aggregation[a]	++++	++	++	+++	++++	++++	++++	++++	+++	++++	+++	++	Fig. 6
Inhibiting secondary nucleation[b]	++++	++++	++	++	++++	++++	++++	++++	++	++	++	++	Fig. 6
Formation of small oligomers[c]	++	+++	++	++++	+++	+++	++++	++++	+++	++	++	++	Fig. S11
Inducing formation of less toxic aggregates to SH-SY5Y cells during fibrillation[d]	++++	+++	++++	++++	++++	++++	++++	++++	++++	++++	++++	++++	Fig. 6

[a] At 0.1 mg/ml of the olive extracts, + denotes 0–25% inhibition, ++ 25–50% inhibition, +++ 50–75% inhibition, and ++++ 75–100% inhibition.
[b] At 0.15 mg/ml of the olive extracts, + denotes 0–25% inhibition, ++ 25–50% inhibition, +++ 50–75% inhibition, and ++++ 75–100% inhibition.
[c] At 0.15 mg/ml of the olive extracts, Min (small oligomer) = A, Max (small oligomer) = B, x = $(A-B)/4$. + denotes A<(small oligomer) $< A + x$, ++ denotes $A + x <$ (small oligomer) $< A + 2x$, +++ denotes $A + 2x <$ (small oligomer) $< A + 3x$, and ++++ denotes $A + 3x <$ (small oligomer) $< B$.
[d] Average of toxicity of aggregates formed over different time ranges compared to control.

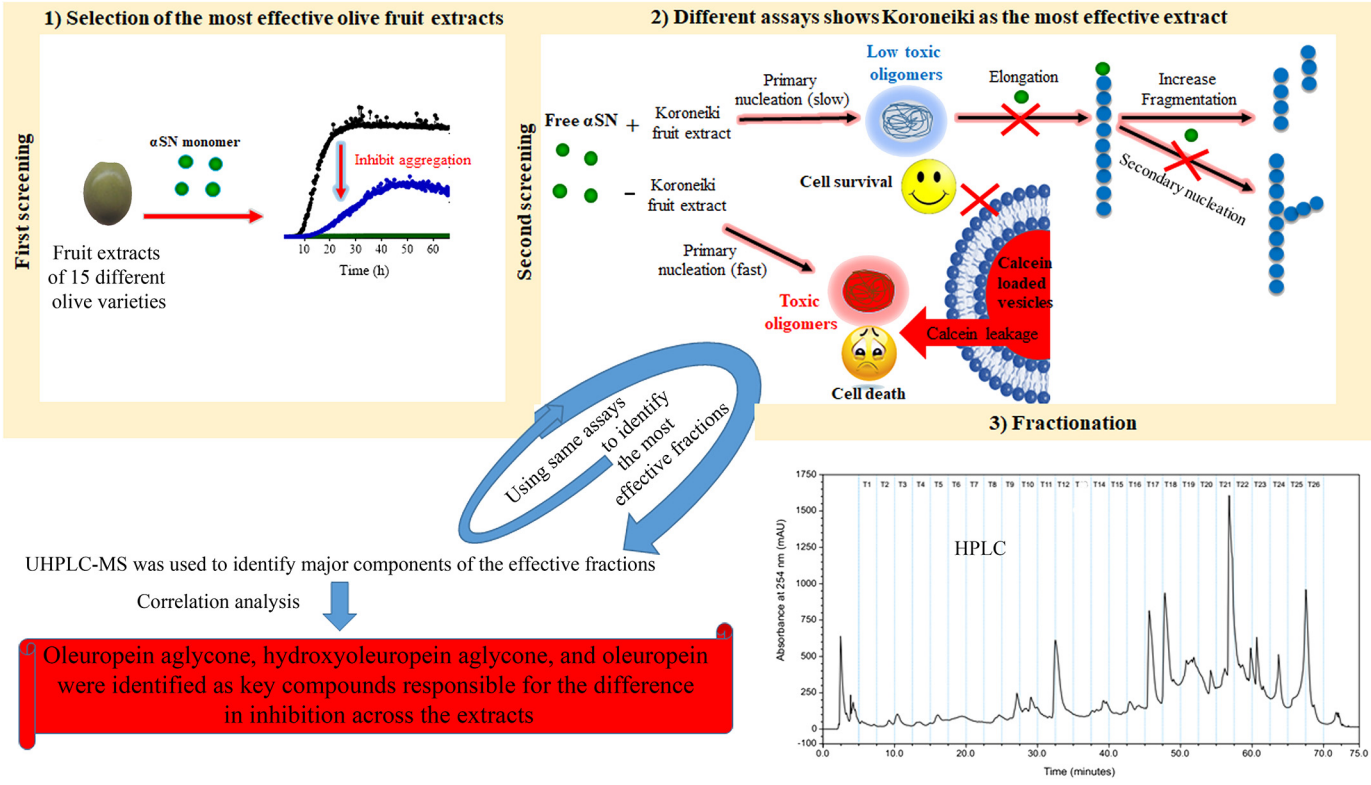

Figure 8. Schematic representation of screening of different olive varieties shown in *panel 1*. The first screening of fruit extract of 15 different olive varieties on the kinetic analysis of αSN fibrillation is shown in *panel 2*. The most effective variety, Koroneiki, combined strong inhibition of αSN fibril nucleation and elongation with a strong ability to disaggregate preformed fibrils and prevent formation of toxic αSN oligomers is shown in *panel 3*. Koroneiki fruit extract was fractionated and by using the same assay as the ones used in step *2*, the most effective fractions were identified. LS-MS analysis was further used to identify the major compounds in the effective fractions. Correlation analysis confirmed oleuropein aglycone, hydroxyl oleuropein aglycone, and oleuropein as key compounds responsible for the difference in inhibition across the extracts.

pounds present in the inhibitory extracts were identified as hydroxytyrosol, hydroxytyrosol glucoside, oleuside, rutine, verbascoside, 6′-(*E*)-*p*-coumaroyl-secologanoside, and compounds structurally related to oleuropein, such as dihydro oleuropein, hydroxyl oleuropein, oleuropein glucoside, hydroxyl oleuropein aglycone, and oleuropein aglycone (Table S3). Some

of these compounds are commercially available and the others can be chemically synthesized or isolated from olive sources. The effects of some of the compounds on fibrillation of proteins and their antioxidant potency have been studied before (22–24). The fractions containing the most effective compounds were ranked in different assays (Table 3). As shown for the extracts, the isolated fractions also have different effects in the assays used in this study (Table 3). Some extracts have more fibrillation inhibitory potency (f5, 19, 20, 21, 22, and 24), some are better in inhibition elongation (f5, 6, 19, 20, 21, and 22), some produce more small oligomers (f18, 21, and 22), some are more effective in disaggregation of preformed fibrils (f5, 20, 24, 25, and 26), and some of them were excellent in decreasing the formation of toxic aggregates (f5, 17, 20, 21, and 26). Interestingly, all the fractions with the highest inhibitory effect (f5, 6, and 17–26) showed higher ROS scavenging ability.

HPLC analysis showed that the content of the polyphenols of olive fruit depends on olive cultivar and ripening stage of the fruit, which leads to a different effect on the fibrillation process and the formed αSN species, antioxidant activity, and ROS scavenging and toxicity. To correlate the change in the polyphenol content of the extracts with their inhibitory effect, we compared the level of the compounds based on the height of the peaks in each extract with the end ThT values in a correlation analysis (Table 1). This analysis shows that oleuropein aglycone, hydroxyl oleuropein aglycone, and oleuropein are the main compounds responsible for the difference in inhibition across the extracts. Koroneiki as the most inhibitory cultivar contains the maximum level of oleuropein aglycone compared with the other varieties. This correlation in the extracts of the same varieties picked at different ripening stages is also clear. Most of the compounds in olive oil result from spontaneous oleuropein hydrolysis and processing (44). The hydrolysis of oleuropein by an endogenous β-glycosidase during ripening leads to formation of oleuropein aglycone, which is the key compound responsible for the protective effect of olive oils. There are other studies on the inhibitory effect of oleuropein aglycone on fibrillation of aggregation-prone proteins. Palazzi *et al.* (27) recently demonstrated that oleuropein aglycone hampers the growth of on-pathway αSN oligomers and favors growth of stable and harmless aggregates. Furthermore, oleuropein aglycone reduces the toxicity of αSN aggregates by interfering with their binding to cell membrane components. These data are in accordance with our own findings that olive compounds rescue cells from the toxicity of αSN aggregates. Oleuropein aglycone also interferes with the *in vitro* aggregation of human amylin and Aβ42 and redirects the aggregation pathway toward nontoxic aggregates, and interferes with Aβ42 proteotoxicity *in vivo* in transgenic *Caenorhabditis elegans* strains expressing Aβ42 by reducing plaque load and motor defect (20, 44, 45).

In summary, we conducted a systematic study of the effect of fruit extracts of different olive varieties on αSN fibrillation, oligomerization, and toxicity, and antioxidant activity to select phenol-rich olive varieties with maximal effective phenolic content to counteract the development of PD hallmarks. We conclude that the polyphenols in olive fruits play a significant role in protection against PD. More specifically, we conclude that polyphenols can reduce αSN aggregate toxicity through their antioxidant activity and direct aggregation toward nontoxic species. Our results contribute to the wider discussions concerning the mechanism of action of polyphenols in aggregation and toxicity prevention. Evaluation of the protection against PD by olive extracts and polyphenols in cell and animal models and development of nanocarriers to increase the bioavailability of olive polyphenols would be an interesting further step to drug development for PD. This will be useful not only for PD but also for assessing the potential of polyphenols in olive oils for future applications.

Experimental procedures

Materials

Penicillin-streptomycin, fetal bovine serum, and Dulbecco's modified Eagle's medium were purchased from Gibco BRL (Gaithersberg, MD). 1,2-Dioleoyl-*sn*-3-phosphatidylglycerol (DOPG) was from Avanti Polar Lipids (Alabaster, AL). The LDH measurement kit was from Pishtazteb Co. (Iran). All other chemicals were from Sigma.

Olive fruit samples

Three distinct categories of olive varieties were studied (Table S1). The first group, the Tarom varieties (T), consists of nine Iranian olive varieties including T10, T15, T16, T17, T18, T20, T22, T23, and T24 (46). The second group consists of three Mediterranean varieties including Koroneiki, Arbequina, and Picual. The third group consists of three major varieties in Iran including Zard, Mari, and Rowghani. All the studied olive trees were nearly 18 years old, reproduced by taking cuttings from the mother plant, irrigated, and fertilized by a drip system at the Tarom olive research station. All trees samples were in the same orchard under the same environmental conditions. Three replicated plants were studied. The fruits were picked at 180 days after full bloom corresponding to different developmental stages for the different olive tree varieties. Samples were stored at −20 °C on the same day of picking (47).

Extraction of phenolic compounds from olive fruits

The fresh mesocarp (3 g) was frozen in liquid nitrogen and ground to fine powder in a porcelain mortar. It was then mixed with methanol (12 ml) and vortexed for 1 min at 20 °C. The resulting mixture was centrifuged (3500 rpm at 4 °C) for 20 min. The supernatant was separated, lyophilized, and stored at −20 °C.

Protein production and purification

Recombinant human αSN was expressed in *Escherichia coli* BL21(DE3) strain with a plasmid vector pET11-D using autoinduction (48). Briefly, the pelleted cells were resuspended in 100 ml of osmotic shock buffer (30 mM Tris-HCl, 40% sucrose, 2 mM EDTA, pH 7.2), and incubated for 10 min followed by centrifugation (9,000 × *g*, 20 °C, 30 min). The resulting pellet was resuspended in 90 ml of ice-cold deionized water and 40 μl of saturated $MgCl_2$ was added, followed by incubation on ice for 3 min. The supernatant after centrifugation (9,000 × *g*, 4 °C, and 20 min) was precipitated by titration with 1 M HCl to pH 3.5 and

then incubated for 5 min. The supernatant was collected by centrifugation (9,000 × *g*, 4 °C, and 20 min) and immediately titrated to pH 7.5 with 1 M NaOH, filtered (0.2 μm) and loaded on a Q-Sepharose column (HiTrap Q H P) pre-equilibrated with 20 mM Tris-HCl, pH 7.5. Then, αSN was eluted with a NaCl gradient from 0.1 to 0.5 M. The fractions were analyzed using SDS-PAGE and the collected purified αSN was dialyzed exhaustively against deionized water, lyophilized, and stored at −20 °C.

Protein and extract handling

Prior to use, freshly dissolved αSN in PBS buffer, pH 7.4, was filtered (0.2 μm). Protein concentration was measured by absorbance measurements at 280 nm with a NanoDrop™ 1000 spectrophotometer (Thermo Scientific) using a theoretical extinction coefficient of 0.412 $(mg/ml)^{-1}$. All olive fruit extracts used in the screening assays were freshly dissolved in PBS buffer and filtered (0.2 μm) prior to use.

Plate reader fibril formation assays

αSN fibril formation was carried out as described (33). Briefly, 150 μl of PBS solution containing 70 μM (1 mg/ml) αSN, 40 μM ThT, and varying amounts of methanolic olive extracts was added to each well of a 96-well plate (Nunc, Thermo Fisher Scientific, Roskilde, Denmark) with a 3-mm diameter glass bead, sealed with crystal clear sealing tape (Hampton Research, Aliso Viejo, CA). The fibrillation was followed at a Genios Pro fluorescence plate reader (Tecan, Männerdorf, Switzerland) at 37 °C with 300 rpm orbital shaking between the readings for 12 min. Samples were excited at 448 nm and emission was measured at 485 nm.

The dose-response aggregation inhibition curves fitted a simple binding isotherm,

$$\mathrm{ThT}_{\text{end level}} = (\mathrm{ThT}_0 - \mathrm{ThT}_{\min})\left(1 - \frac{[\text{olive extract}]}{K_D + [\text{olive extract}]}\right) + \mathrm{ThT}_{\min} \quad \text{(Eq. 1)}$$

where $\mathrm{ThT}_{\text{end level}}$ is the ThT fluorescence level at the end of the fibrillation process at a given olive concentration, ThT_0 is the ThT fluorescence end level in the absence of compounds, $\mathrm{ThT}_{\min}$ represents the ThT level at maximum inhibition, [olive extract] is the concentration of the olive extract, and K_D is the mole ratio needed for half-inhibition.

The Finke-Watzky (F-W) (49) equation was fitted to the normalized ThT fibrillation data,

$$F(t) = \frac{1}{1 + e^{-4\nu(t - t_{1/2})}} \quad \text{(Eq. 2)}$$

$$t_N = t_{1/2} - \frac{1}{2\nu} \quad \text{(Eq. 3)}$$

where $t_{½}$ is the time required to produce half the total product, ν is the rate of growth at $t_{½}$ and t_N is the duration of the nucleation (lag) phase (31).

Seeding experiments

The fibril elongation assays were performed using a plate reader setup with the same settings as for the fibrillation assay in the presence of 0.05 mg/ml of seeds (corresponding to 3.5 μM monomer) and 0.15 mg/ml of olive extracts in a solution of 70 μM monomeric αSN in 96-well plates. The snap-frozen mature fibrils were thawed and fragmented by sonication for 2 min on ice (pulse 5-s on and 5-s off) with an amplitude of 20% on a QSonica Sonicators (Q500, Newtown, CT) to obtain short fibrils, which were employed as seeds.

Fibril disaggregation assays

The fibril stock solution was prepared using the same setting as for the fibrillation assay and the fibrils. Aggregated αSN (35 μM monomer equivalents) was incubated overnight either alone or with the olive extracts (0.15 mg/ml) at 37 °C. The solution was centrifuged (21,000 × *g*, 20 min) and the supernatant was injected onto a 24-ml Superose 6 10/300 gel filtration column (GE Healthcare Lifescience) at 0.5 ml/min to separate monomers and oligomeric species.

Preparation of oligomers

αSN oligomers were prepared as previously described (16). Briefly, 12 mg/ml of αSN was incubated in PBS buffer for 5 h at 37 °C and 900 rpm on an Eppendorf thermoshaker, TS-100 (BioSan, Latvia). The sample was then centrifuged (21,000 × *g*, 10 min) to remove insoluble material and the supernatant was loaded on an a Superose 6 Prep Grade column (GE Healthcare Life Sciences, Sweden) in PBS at 2.5 ml/min. Small oligomers were collected and were concentrated with 15-ml Amicon ultracentrifugal filters (Merck).

Preparation of large unilamellar vesicles

Large unilamellar vesicles were prepared as described (50). Briefly, DOPG or 1,2-dimyristoyl-*sn*-glycero-3-phospho-(1′-rac-glycerol) (sodium salt) (DMPG) was dissolved at 5 mg/ml in PBS. The solution was subjected to 10 freeze-thaw cycles between liquid nitrogen and a 50 °C water bath. The lipid solution was extruded 21 times through a 100-nm filter. To prepare calein-loaded vesicles, calcein at self-quenching concentrations (70 mM) was added to the phospholipids and after extrusion, the vesicle solution was run through a PD-10 desalting column (GE Healthcare) to separate free calcein from calcein-loaded vesicles.

Analyzing soluble αSN remaining in solution

To analyze soluble αSN remaining in the solution, samples were taken from the plate after 24 h incubation and pelleted by centrifugation for 10 min at 21,000 × *g*. This speed can pellet large fibrillar aggregates, leaving in the supernatant monomers and oligomers that do not even pellet during ultracentrifugation unless bound to, *e.g.* phospholipid vesicles (51). We are able to discriminate monomers and oligomers by SDS-PAGE because the latter are SDS-resistant (10). The supernatant was mixed with SDS-PAGE sample loading buffer and heated for 2 min at 95 °C before loading on a 15% SDS-PAGE gel. The supernatant was also run on a Superose 6_10/300 gel filtration column.

Circular dichroism (CD) spectroscopy

For far-UV CD, sonicated fibril solutions with a protein concentration of 0.2 mg/ml (14 μM) were placed in a 1-mm cuvette and the spectra were measured from 250 to 195 nm at 25 °C with a Jasco J-810 spectrophotometer (Jasco Spectroscopic Co. Ltd., Japan). To measure the induced changes in the secondary structure of αSN by DMPG vesicles and the effect of olive samples on this interaction, 0.2 mg/ml (14 μM) of αSN was mixed with 0.2 mg/ml of DMPG vesicles in the presence and absence of 0.15 mg/ml of olive samples in PBS buffer at 37 °C. CD spectra of PBS buffer and the olive solutions were recorded and subtracted from the protein spectra and the CD signal given as mean residue ellipticity (degrees cm^2 $dmol^{-1}$).

TEM

αSN sample in 5 μl of PBS buffer was transferred to a carbon-coated, glow-discharged 400-mesh grid for 30 s. The grids were washed using 2 drops of double distilled water, stained with 1% (w/v) phosphotungstic acid, pH 6.8, and blotted dry. The samples were viewed in a microscope (JEM-1010; JEOL, Tokyo, Japan) operating at 60 kV. Images were obtained using an Olympus KeenView G2 camera.

Oligomerization assays

αSN monomer (1 mg/ml) was incubated on an Eppendorf TS-100 thermoshaker (BioSan) with 0.15 mg/ml of olive extracts for 1 h at 37 °C and 900 rpm. The solution was centrifuged (21,000 × *g*, 20 min) and the supernatant was injected into a 24-ml Superose 6 10/300 gel filtration column at 0.5 ml/min. Samples from both oligomerization and disaggregation assays were run on an SEC-MALS system (Wyatt Technology Europe) using separation on a Superose 6_10/300 gel filtration column and analyzed using 18-angle static laser light scattering (Dawn Heleos II), refractive index (Optilab T-rEX differential refractometer), and absorbance at 280 nm (Agilent 1260 Analytical UV cell). Data were collected and analyzed using the software ASTRA 6.1.7.17 (Wyatt Technology Europe).

Calcein release assays

The membrane permeabilization assay was carried out to compare the membrane-disrupting ability of different αSN aggregates that form in the presence and absence of the extracts. Oligomers permeabilize the membrane (and by inference induce toxicity in cells) much more efficiently than fibrils. Permeabilization of vesicles due to the interaction with oligomers results in calcein release and an increase in the fluorescence signal due to dilution. Calcein-loaded DOPG vesicles at a final lipid concentration of 42 μM were loaded in triplicate in a 140-μl assay solution onto a 96-well plate (Nunc, Thermo Fisher Scientific). The background fluorescence at excitation 485 nm and emission at 520 nm was measured on a Genios Pro fluorescence plate reader (Tecan, Männerdorf, Switzerland) before and after addition of vesicles. The olive extracts and/or oligomers at a final concentration of 0.02– 0.2 mg/ml and 0.5 μM, respectively, were mixed with vesicles in a final volume of 150 μl. The plates were sealed with crystal clear sealing tape (Hampton Research) and calcein release was measured for 1 h at 37 °C every 1.5 min with 2-s autoshake before each reading. Finally, 1 μl of Triton X-100 (0.1% (w/v)) was added to lyse vesicles, leading to complete calcein release and maximal fluorescence signal. Background fluorescence was subtracted.

HPLC analysis of phenolic compounds in different olive fruit extracts

The extracts were analyzed with an Ultimate 3000 model HPLC, run on a RP-C18 Luna column, 4.6-mm inner diameter × 250 mm and particle size 5 μm (Phenomenex, UK). For each injection (50 μl), elution was performed at a flow rate of 1 ml/min, using a solvent system of water/TFA (1%) (A) and acetic acid/TFA (1%) (B). Elution was started with 5% B, and continued with a gradient to 35% B at 45 min, 90% B at 55 to 57 min, and then reduced to 5% B at 61 min. Chromatograms were recorded at 230 nm.

Fractionation of Koroneiki extracts by HPLC

Dried extracts were reconstituted using 1.75 ml of water. Fractionation was carried out using an HPLC system (Dionex UltiMate 3000, Thermo Fisher Scientific) equipped with an Ascentis C-18 column (5 μm, 5 × 250 mm, Supelco, UK). Chromatographic separation was performed using a constant flow rate of 1 ml/min of the mobile phases water, 0.1% formic acid (A) and acetonitrile, 0.1% formic acid (B). The binary gradient was: 0–10 min, 5% B; 10–50 min, 22% B; 50–60 min, 37% B; and finally 60–70 min, 50% B. Fractions were collected every 2.5 min between 5 and 70 min (T1–T26). Twelve injections (100 μl each) were performed and fractions from repeated runs were combined. Thirty μl of each fraction was diluted with 270 μl of 80/20 (v/v) water/methanol and subsequently analyzed by UHPLC-MS. The remainder of each fraction was dried using a SpeedVac concentrator (Genevac, Suffolk, UK).

Identification of phenolic compounds in Koroneiki extract fractions by UHPLC-MS

To identify the compounds, UHPLC-MS were recorded with an Ultimate 3000 RS UHPLC system, equipped with a DAD-3000 photodiode array detector, coupled to an LTQ-Orbitrap Elite mass spectrometer (Thermo Scientific, Germany). An injection volume of 10 μl was used and the elution was performed on a reversed-phase C18 Hypersil gold column (1.9 μm, 30 × 2.1-mm inner diameter, Thermo, Hemel Hempstead, UK), at 35 °C, using a solvent system consisting of water, 0.1% formic acid (A) and acetonitrile, 0.1% formic acid (B) under the following conditions: 0–5 min, 0% B; 5–27 min, 31.6% B; 27–34 min, 45% B; 34–37.5 min, 75% B at a flow rate of 0.3 ml/min. Mass spectra were collected using an LTQ-Orbitrap Elite with a heated ESI source (Thermo Scientific). Mass spectra were acquired in negative mode with a resolution of 120,000 over m/z 50–1500. The source voltage, sheath gas, auxiliary gas, sweep gas, and capillary temperature were set to 2.5 kV, 35 (arbitrary units), 10 (arbitrary units), 0.0 (arbitrary units), and 350 °C, respectively. Default values were used for other acquisition parameters. Automatic MS-MS was performed on the 4 most abundant ions using an isolation width of m/z 2. Ions were fragmented using high-energy C-trap dissociation (HCD) with

a normalized collision energy of 65 and an activation time of 0.1 ms. Data analysis was carried out using Xcalibur version 2.2 (Thermo Scientific). Compounds were identified on the basis of their retention time, accurate mass, and MS-MS fragmentation patterns. Where possible, known compounds were compared with authentic standards if available. Where this was not possible, a comparison to the reported MS-MS fragmentation data were made for known compounds. Compounds where structural data could not be verified were labeled as unknown. A full table of the LC-MS data were prepared, including details of identification method for each component and reference data for known compounds (Table S2).

Antioxidant activity

The antioxidant activity of the olive extracts was determined by monitoring the disappearance of DPPH$^{\bullet}$ in the presence of olive extracts at 517 nm. Olive extracts (20 μl) at various concentrations was mixed with 200 μl of DPPH$^{\bullet}$ solution (0.135 mM). The resulting medium was incubated at room temperature in darkness for 30 min. The antioxidant activity was determined using the following formula.

$$\text{Antioxidant activity} = (\text{Abs}_{517}{}^{\text{control}} - \text{Abs}_{517}{}^{\text{sample}})/\text{Abs}_{517}{}^{\text{control}} \times 100 \quad \text{(Eq. 4)}$$

ROS assay

To assess whether olive extracts interfered with the level of ROS within the cells, 2′,7′-dichlorodihydrofluorescein diacetate (DCFH-DA) was used. OLN-93 cells were seeded in 96-well plates at a density of 6×10^4 cells/ml and incubated in a humidified atmosphere incubator at 37 °C for 24 h. The medium was then removed and the cells washed with PBS and replaced by PBS containing 15 μM DCFH-DA. The plate was incubated for 45 min in the dark in a CO_2 incubator. DCFH-DA was removed and the wells were washed with PBS, treated with culture medium containing olive extracts in the absence or presence of 100 μM H_2O_2, and incubated at 37 °C (for 1 h) after which fluorescence of DCF was recorded in a microtiter plate reader (excitation/emission: 490/527 nm).

Evaluation of cell viability

The MTT assay was implemented to measure cellular viability after 24 h treatment by monomeric or aggregated forms of αSN. OLN-93 and SH-SY5Y cells were seeded in 96-well plates at concentrations of 30×10^3 and 60×10^3 cells/ml, respectively, in Dulbecco's modified Eagle's medium supplemented with 10% (v/v) fetal bovine serum, 100 units/ml of penicillin, and 100 μg/ml of streptomycin and cultured for 24 h. The medium was then replaced with fresh medium containing different concentrations of olive extracts or with 12.5% αSN samples (collected during the fibrillation process). After 24 h at 37 °C, the old medium was replaced with fresh medium containing 10% MTT (5 mg/ml), and the plates were incubated for an additional 4 h at 37 °C. To avoid possible interference between antioxidant compounds and the MTT assay, the cells were washed to remove aggregates and compounds before adding MTT. The formazan crystals were dissolved in 100 μl of DMSO by incubating for 1 h on a shaking table at room temperature. Finally, absorbance was determined by a plate reader at 570 nm using 650 nm as a reference wavelength. Cell viability was calculated as follows.

$$\text{Cell viability (\%)} = (\text{Abs}_{570}\,(\text{treated cells})/\text{Abs}_{570}\,(\text{control cells}) \times 100 \quad \text{(Eq. 5)}$$

LDH assay

Release of cytoplasmic enzyme, LDH, as the sign of loss of membrane integrity was measured. After treatment of the cells with αSN samples, 100 μl of growth medium was added to 1 ml of the kit substrate and absorbance at 340 nm was determined for 4 min to follow the conversion of NADH to NAD^+. The values were expressed as a percentage of the untreated cells as control.

Analysis of HPLC elution profiles

The average values of the end ThT values of αSN aggregation in the presence of different concentrations of olive extracts and HPLC data of the olive extracts were used to analyze the effect of different compounds in the olive fruit extracts. The peakutils Python package (10.5281/zenodo.887917) was used to identify peaks in the HPLC data and the "sklearn" Python package (http://scikit-learn.org/stable/)[7] to cluster them as follows. (a) The threshold for identifying peaks (the minimum height) was set to 750 absorbance units. (*b*) The minimum distance between peaks was set to 50 data points. (*c*) All of the peaks identified in this way (across all of the datasets) were compiled into a single list of peaks, and a *k*-means clustering was used to cluster the peaks into 5 groups. (*d*) The cluster centers were extracted and used to identify the peaks in further analyses.

For each peak that was identified, a relative measure of the "amount of compound" in each sample was determined by multiplying the concentration of the extract (mg/ml) by the height of the peak. Where the data were available, the amount of compound was plotted against the ThT signal. Data points with ThT signals below 1000 (arbitrary unit) were excluded from further analysis under the assumption that these corresponded to maximal inhibition and therefore might obscure attempts to determine whether the concentration of the compound was related to the level of the ThT signal in the relevant range (between 7000 and 1000 units). For each compound, the coefficient of determination (R^2), and Spearman's rank correlation coefficient were computed, and an isotonic regression model was built from the data. The R^2 value measures the goodness of fit assuming a linear model, whereas the Spearman's rank correlation coefficient measures how monotonically related the two quantities are without making an assumption about the functional form of the relationship. *R*-squared values are always positive and between 0 and 1. Spearman *R* values can be in the range of −1 to 1. The isotonic regression generates an optimal monotonic fit to the data. The slope of the optimal linear fit (the m-value) was taken a measure of potency, with larger (negative)

[7] Please note that the JBC is not responsible for the long-term archiving and maintenance of this site or any other third party hosted site.

slopes corresponding to more potent inhibition. Finally, a correlation analysis was performed to determine which peaks had correlated amounts across all of the samples.

Statistical analysis

Data were obtained in triplicate and averaged. The results are shown as mean ± S.D. Statistical differences between group means were analyzed by analysis of variance. A value of $p < 0.05$ was considered statistically significant.

Author contributions—H. M.-B. conceived and designed the experiments, wrote the manuscript, and analyzed the data; F. A., C. S., C. L., A. T., N. P. S., A. A.-N., and H. E. performed the experiments; I. M. M., M. H.-M., and J. L. W. contributed reagents/materials/analysis tools; G. C. contributed reagents/materials/analysis tools, performed the experiments; D. M. conceived and designed the experiments; D. E. O. conceived and designed the experiments, analyzed the data, and wrote the manuscript.

References

1. Hardy, J., Cookson, M. R., and Singleton, A. (2003) Genes and parkinsonism. *Lancet Neurol.* **2,** 221–228 CrossRef Medline
2. Spillantini, M. G., Schmidt, M. L., Lee, V. M.-Y., Trojanowski, J. Q., Jakes, R., and Goedert, M. (1997) α-Synuclein in Lewy bodies. *Nature* **388,** 839–840 CrossRef Medline
3. Jakes, R., Spillantini, M. G., and Goedert, M. (1994) Identification of two distinct synucleins from human brain. *FEBS Lett.* **345,** 27–32 CrossRef Medline
4. Masuda-Suzukake, M., Nonaka, T., Hosokawa, M., Oikawa, T., Arai, T., Akiyama, H., Mann, D. M., and Hasegawa, M. (2013) Prion-like spreading of pathological α-synuclein in brain. *Brain* **136,** 1128–1138 CrossRef Medline
5. Van Rooijen, B., van Leijenhorst-Groener, K. A., Claessens, M. M., and Subramaniam, V. (2009) Tryptophan fluorescence reveals structural features of α-synuclein oligomers. *J. Mol. Biol.* **394,** 826–833 CrossRef Medline
6. Fauvet, B., Mbefo, M. K., Fares, M.-B., Desobry, C., Michael, S., Ardah, M. T., Tsika, E., Coune, P., Prudent, M., Lion, N. *et al.* (2012) α-Synuclein in central nervous system and from erythrocytes, mammalian cells, and *Escherichia coli* exists predominantly as disordered monomer. *J. Biol. Chem.* **287,** 15345–15364 Medline CrossRef
7. Paslawski, W., Mysling, S., Thomsen, K., Jørgensen, T. J., and Otzen, D. E. (2014) Co-existence of two different α-synuclein oligomers with different core structures determined by hydrogen/deuterium exchange mass spectrometry. *Angew. Chem. Int. Ed.* **53,** 7560–7563 CrossRef Medline
8. Ingelsson, M. (2016) α-Synuclein oligomers: neurotoxic molecules in Parkinson's disease and other Lewy body disorders. *Front. Neurosci.* **10,** 408 Medline
9. Fink, A. L. (2006) in *Misbehaving Proteins,* pp. 265–285, Springer, New York
10. Paslawski, W., Andreasen, M., Nielsen, S. B., Lorenzen, N., Thomsen, K., Kaspersen, J. D., Pedersen, J. S., and Otzen, D. E. (2014) High stability and cooperative unfolding of α-synuclein oligomers. *Biochemistry* **53,** 6252–6263 CrossRef Medline
11. Prots, I., Veber, V., Brey, S., Campioni, S., Buder, K., Riek, R., Böhm, K. J., and Winner, B. (2013) α-Synuclein oligomers impair neuronal microtubule-kinesin interplay. *J. Biol. Chem.* **288,** 21742–21754 CrossRef
12. Chen, L., Jin, J., Davis, J., Zhou, Y., Wang, Y., Liu, J., Lockhart, P. J., and Zhang, J. (2007) Oligomeric α-synuclein inhibits tubulin polymerization. *Biochem. Biophys. Res. Commun.* **356,** 548–553 CrossRef Medline
13. Nakamura, K. (2013) α-Synuclein and mitochondria: partners in crime? *Neurotherapeutics* **10,** 391–399 CrossRef Medline
14. Nakamura, K., Nemani, V. M., Azarbal, F., Skibinski, G., Levy, J. M., Egami, K., Munishkina, L., Zhang, J., Gardner, B., Wakabayashi, J., and others. (2011) Direct membrane association drives mitochondrial fission by the Parkinson disease-associated protein α-synuclein. *J. Biol. Chem.* **286,** 20710–20726 CrossRef
15. Angelova, P. R., and Abramov, A. Y. (2018) Role of mitochondrial ROS in the brain: from physiology to neurodegeneration. *FEBS Lett.* **592,** 692–702 CrossRef Medline
16. Lorenzen, N., Nielsen, S. B., Yoshimura, Y., Vad, B. S., Andersen, C. B., Betzer, C., Kaspersen, J. D., Christiansen, G., Pedersen, J. S., Jensen, P. H., *et al.* (2014) How epigallocatechin gallate can inhibit α-synuclein oligomer toxicity *in vitro*. *J. Biol. Chem.* **289,** 21299–21310 24907278 CrossRef
17. Keys, A., Mienotti, A., Karvonen, M. J., Aravanis, C., Blackburn, H., Buzina, R., Djordjevic, B. S., Dontas, A. S., Fidanza, F., Keys, M. H., *et al.* (1986) The diet and 15-year death rate in the seven countries study. *Am. J. Epidemiol.* **124,** 903–915 CrossRef Medline
18. Gaskins, A. J., Rovner, A. J., Mumford, S. L., Yeung, E., Browne, R. W., Trevisan, M., Perkins, N. J., Wactawski-Wende, J., Schisterman, E. F., and BioCycle Study Group (2010) Adherence to a Mediterranean diet and plasma concentrations of lipid peroxidation in premenopausal women. *Am. J. Clin. Nutr.* **92,** 1461–1467 CrossRef Medline
19. Dai, J., Jones, D. P., Goldberg, J., Ziegler, T. R., Bostick, R. M., Wilson, P. W., Manatunga, A. K., Shallenberger, L., Jones, L., and Vaccarino, V. (2008) Association between adherence to the Mediterranean diet and oxidative stress. *Am. J. Clin. Nutr.* **88,** 1364–1370 Medline
20. Casamenti, F., and Stefani, M. (2017) Olive polyphenols: new promising agents to combat aging-associated neurodegeneration. *Expert Rev. Neurother.* **17,** 345–358 Medline
21. Tripoli, E., Giammanco, M., Tabacchi, G., Di Majo, D., Giammanco, S., and La Guardia, M. (2005) The phenolic compounds of olive oil: structure, biological activity and beneficial effects on human health. *Nutr. Res. Rev.* **18,** 98–112 CrossRef Medline
22. Rigacci, S., Guidotti, V., Bucciantini, M., Nichino, D., Relini, A., Berti, A., and Stefani, M. (2011) Aβ(1–42) aggregates into non-toxic amyloid assemblies in the presence of the natural polyphenol oleuropein aglycon. *Curr. Alzheimer Res.* **8,** 841–852 CrossRef Medline
23. Daccache, A., Lion, C., Sibille, N., Gerard, M., Slomianny, C., Lippens, G., and Cotelle, P. (2011) Oleuropein and derivatives from olives as Tau aggregation inhibitors. *Neurochem. Int.* **58,** 700–707 CrossRef Medline
24. Caruana, M., Högen, T., Levin, J., Hillmer, A., Giese, A., and Vassallo, N. (2011) Inhibition and disaggregation of α-synuclein oligomers by natural polyphenolic compounds. *FEBS Lett.* **585,** 1113–1120 CrossRef Medline
25. Ahmad, E., Ahmad, A., Singh, S., Arshad, M., Khan, A. H., and Khan, R. H. (2011) A mechanistic approach for islet amyloid polypeptide aggregation to develop anti-amyloidogenic agents for type-2 diabetes. *Biochimie (Paris)* **93,** 793–805 CrossRef
26. Wu, C., Lei, H., Wang, Z., Zhang, W., and Duan, Y. (2006) Phenol red interacts with the protofibril-like oligomers of an amyloidogenic hexapeptide NFGAIL through both hydrophobic and aromatic contacts. *Biophys. J.* **91,** 3664–3672 CrossRef Medline
27. Palazzi, L., Bruzzone, E., Bisello, G., Leri, M., Stefani, M., Bucciantini, M., and Polverino de Laureto, P. (2018) Oleuropein aglycone stabilizes the monomeric α-synuclein and favours the growth of non-toxic aggregates. *Sci. Rep.* **8,** 8337 CrossRef Medline
28. Omar, S. H., Scott, C. J., Hamlin, A. S., and Obied, H. K. (2018) Biophenols: enzymes (Aβ-secretase, cholinesterases, histone deacetylase and tyrosinase) inhibitors from olive (*Olea europaea* L.). *Fitoterapia* **128,** 118–129 CrossRef Medline
29. Servili, M., and Montedoro, G. (2002) Contribution of phenolic compounds to virgin olive oil quality. *Eur. J. Lipid Sci. Technol.* **104,** 602–613 CrossRef
30. Petridis, A., Therios, I., and Samouris, G. (2012) Genotypic variation of total phenol and Oleuropein concentration and antioxidant activity of 11 Greek olive cultivars (*Olea europaea* L.). *HortScience* **47,** 339–342 CrossRef
31. Romero, C., Medina, E., Mateo, M. A., and Brenes, M. (2017) Quantification of bioactive compounds in Picual and Arbequina olive leaves and fruit. *J. Sci. Food Agric.* **97,** 1725–1732 CrossRef Medline

32. Vossen, P. (2007) Olive oil: history, production, and characteristics of the world's classic oils. *HortScience* **42,** 1093–1100
33. Giehm, L., and Otzen, D. E. (2010) Strategies to increase the reproducibility of protein fibrillization in plate reader assays. *Anal. Biochem.* **400,** 270–281 CrossRef Medline
34. Lorenzen, N., Nielsen, S. B., Buell, A. K., Kaspersen, J. D., Arosio, P., Vad, B. S., Paslawski, W., Christiansen, G., Valnickova-Hansen, Z., Andreasen, M., Enghild, J. J., Pedersen, J. S., Dobson, C. M., Knowles, T. P., and Otzen, D. E. (2014) The role of stable α-synuclein oligomers in the molecular events underlying amyloid formation. *J. Am. Chem. Soc.* **136,** 3859–3868 CrossRef Medline
35. Kjaer, L., Giehm, L., Heimburg, T., and Otzen, D. (2009) The influence of vesicle size and composition on α-synuclein structure and stability. *Biophys. J.* **96,** 2857–2870 CrossRef Medline
36. Perni, M., Galvagnion, C., Maltsev, A., Meisl, G., Müller, M. B., Challa, P. K., Kirkegaard, J. B., Flagmeier, P., Cohen, S. I., Cascella, R., *et al.* (2017) A natural product inhibits the initiation of α-synuclein aggregation and suppresses its toxicity. *Proc. Natl. Acad. Sci. U.S.A.* **114,** E1009–E1017 CrossRef
37. Aliakbari, F., Shabani, A., Bardania, H., Seyedi, E., Alsadat, H., Mohammad-Beigi, H., Tayaranian Marvian, A., Nassoti, M., Vafaei, A. A., Shojaosadati, S. A., *et al.* (2017) Neurotoxicity of pre-incubated α-synuclein with neutral nanoliposomes on PC12 and SHSY5Y cell lines. *Scientia Iranica* **24,** 3542–3553
38. Zhao, J., Liang, Q., Sun, Q., Chen, C., Xu, L., Ding, Y., and Zhou, P. (2017) (−)-Epigallocatechin-3-gallate (EGCG) inhibits fibrillation, disaggregates amyloid fibrils of α-synuclein, and protects PC12 cells against α-synuclein-induced toxicity. *Rsc Advances* **7,** 32508–32517 CrossRef
39. Vossen, P. M. (2007) *Organic olive production manual*, University of California Agriculture and Natural Resources Communication Services (UCANR), Davis, CA
40. Mohammad-Beigi, H., Morshedi, D., Shojaosadati, S. A., Pedersen, J. N., Marvian, A. T., Aliakbari, F., Christiansen, G., Pedersen, J. S., and Otzen, D. E. (2016) Gallic acid loaded onto polyethylenimine-coated human serum albumin nanoparticles (PEI-HSA-GA NPs) stabilizes α-synuclein in the unfolded conformation and inhibits aggregation. *Rsc Advances* **6,** 85312–85323 CrossRef
41. Souza, J. M., Giasson, B. I., Chen, Q., Lee, V. M.-Y., and Ischiropoulos, H. (2000) Dityrosine cross-linking promotes formation of stable α-synuclein polymers implication of nitrative and oxidative stress in the pathogenesis of neurodegenerative synucleinopathies. *J. Biol. Chem.* **275,** 18344–18349 CrossRef
42. Abou-Sleiman, P. M., Muqit, M. M., and Wood, N. W. (2006) Expanding insights of mitochondrial dysfunction in Parkinson's disease. *Nat. Rev. Neurosci.* **7,** 207–219 CrossRef Medline
43. Mandel, S., and Youdim, M. B. (2004) Catechin polyphenols: neurodegeneration and neuroprotection in neurodegenerative diseases. *Free Radic. Biol. Med.* **37,** 304–317 CrossRef Medline
44. Diomede, L., Rigacci, S., Romeo, M., Stefani, M., and Salmona, M. (2013) Oleuropein aglycone protects transgenic *C. elegans* strains expressing Aβ42 by reducing plaque load and motor deficit. *PLoS One* **8,** e58893 CrossRef Medline
45. Rigacci, S., Guidotti, V., Bucciantini, M., Parri, M., Nediani, C., Cerbai, E., Stefani, M., and Berti, A. (2010) Oleuropein aglycon prevents cytotoxic amyloid aggregation of human amylin. *J. Nutr. Biochem.* **21,** 726–735 CrossRef Medline
46. Hosseini-Mazinani, M., Torkzaban, B., and Arab, J. (2013) Iranian olive catalogue: morphological and molecular characterization of Iranian olive germplasm. *NIGEB*, Tehran, Iran CrossRef
47. Amiri-Nowdijeh, A., Fazelipour, F., Haghbeen, K., Taheri, M., *et al.* (2018) Minor olive varieties from Iran with promising nutraceutical properties. *J. Agr. Sci. Technol.* **20,** 347–357
48. Mohammad-Beigi, H., Shojaosadati, S. A., Marvian, A. T., Pedersen, J. N., Klausen, L. H., Christiansen, G., Pedersen, J. S., Dong, M., Morshedi, D., and Otzen, D. E. (2015) Strong interactions with polyethylenimine-coated human serum albumin nanoparticles (PEI-HSA NPs) alter α-synuclein conformation and aggregation kinetics. *Nanoscale* **7,** 19627–19640 CrossRef Medline
49. Morris, A. M., Watzky, M. A., Agar, J. N., and Finke, R. G. (2008) Fitting neurological protein aggregation kinetic data via a 2-step, minimal "Ockham's razor" model: the Finke-Watzky mechanism of nucleation followed by autocatalytic surface growth. *Biochemistry* **47,** 2413–2427 CrossRef Medline
50. Nesgaard, L., Vad, B., Christiansen, G., and Otzen, D. (2009) Kinetic partitioning between aggregation and vesicle permeabilization by modified ADan. *Biochim. Biophys. Acta* **1794,** 84–93 CrossRef Medline
51. Sahin, C., Lorenzen, N., Lemminger, L., Christiansen, G., Møller, I. M., Vesterager, L. B., Pedersen, L. Ø, Fog, K., Kallunki, P., and Otzen, D. E. (2017) Antibodies against the C-terminus of α-synuclein modulate its fibrillation. *Biophys. Chem.* **220,** 34–41 CrossRef Medline